

Probing spectral features of quantum many-body systems with quantum simulators

Jinzhao Sun,^{1,2,*} Lucia Vilchez-Estevez,^{1,†} Vlatko Vedral,¹ Andrew T. Boothroyd,¹ and M. S. Kim²

¹*Clarendon Laboratory, University of Oxford, Parks Road, Oxford OX1 3PU, United Kingdom*

²*Blackett Laboratory, Imperial College London, London SW7 2AZ, United Kingdom*

(Dated: February 11, 2025)

The efficient probing of spectral features is important for characterising and understanding the structure and dynamics of quantum materials. In this work, we establish a framework for probing the excitation spectrum of quantum many-body systems with quantum simulators. Our approach effectively realises a spectral detector by processing the dynamics of observables with time intervals drawn from a defined probability distribution, which only requires native time evolution governed by the Hamiltonian without ancilla. The critical element of our method is the engineered emergence of frequency resonance such that the excitation spectrum can be probed. We show that the time complexity for transition energy estimation has a logarithmic dependence on simulation accuracy and how such observation can be guaranteed in certain many-body systems. We discuss the noise robustness of our spectroscopic method and show that the total running time maintains polynomial dependence on accuracy in the presence of device noise. We further numerically test the error dependence and the scalability of our method for lattice models. We present simulation results for the spectral features of typical quantum systems, either gapped or gapless, including quantum spins, fermions and bosons. We demonstrate how excitation spectra of spin-lattice models can be probed experimentally with IBM quantum devices.

I. INTRODUCTION

Estimating spectral features of quantum many-body systems has attracted great attention in condensed matter physics and quantum chemistry. To achieve this task, various experimental and theoretical techniques have been developed, such as spectroscopy techniques [1–7] and quantum simulation either by engineering controlled quantum devices [8–16] or executing quantum algorithms [17–21] such as quantum phase estimation and variational algorithms. However, probing the behaviour of complex quantum many-body systems remains a challenge, which demands substantial resources for both approaches. For instance, a real probe by neutron spectroscopy requires access to large-scale facilities with high-intensity neutron beams, while quantum computation of eigenenergies typically requires controlled operations with a long coherence time [17, 18]. Efficient estimation of spectral properties has become a topic of increasing interest in this noisy intermediate-scale quantum era [22].

A potential solution to efficient spectral property estimation is to extract the spectral information from the dynamics of observables, rather than relying on real probes such as scattering spectroscopy, or direct computation of eigenenergies. This approach capitalises on the basics in quantum mechanics that spectral information is naturally carried by the observable’s dynamics [10, 20, 23–27]. In a solid system with translation invariance, for instance, the dynamic structure factor, which can be probed in spectroscopy experiments [7, 27], reaches its local maximum when both the energy and

momentum selection rules are satisfied. Therefore, the energy dispersion can be inferred by tracking the peak of intensities in the energy excitation spectrum. Inspired by spectroscopy, a straightforward way to detect spectral features of model systems is by directly simulating spectroscopy [16, 20, 27, 28] using quantum computers, which often requires the measurement of an unequal-time correlator on a thermal state with long-time evolution. Another similar idea is to extract spectral information by post-processing the time-dependent signals [10, 23–26, 29–32] which is usually ancilla-free. For example, Zintchenko and Wiebe [30] proposed to estimate the spectral gap by using Bayesian inference of the measurement outcomes generated by applying random unitaries (see other similar works [31, 32]). Wang *et al.* [33, 34] and Stenger *et al.* [35] proposed detecting energy differences by measuring the dynamical response of a quantum system when coupled to a probe qubit. Recently, Chan *et al.* proposed to perform the Fourier transform of observable’s dynamics and innovatively use shadows [36] to estimate many observables simultaneously [26] (see other relevant works [10, 23–25, 37]). Nevertheless, methods that extract spectral information from dynamics face challenges in achieving high-precision results with short-time dynamics. In addition, it is generally hard to design appropriate spectroscopic protocols for many-body systems. A pressing question is whether we can probe the spectral features and obtain high-precision results with fewer quantum resources.

In this work, we introduce a spectroscopic method that links spectroscopy techniques and quantum simulation while addressing the above challenges in probing transition energies and excitation spectra. We show how a spectral detector can be effectively realised by processing the dynamics of observables with time intervals drawn

* jinzhao.sun.phys@gmail.com

† lucia.vilchezestevez@physics.ox.ac.uk

from a defined probability distribution. The maximum time complexity is found to be logarithmic in precision under assumptions similar to those used in eigenenergy estimation [38–43], which enables high-precision simulation with short-time dynamics. The essential requirement of the spectroscopic method is a nonvanishing observation of the target transitions between eigenstates, which depends on the initial state and the observable. We illustrate how this nonvanishing observation can be guaranteed in some representative many-body systems with quasiparticle number conservation. In terms of practical implementation, our method only requires the realisation of time evolution e^{-iHt} , in contrast to existing algorithms for eigenenergy estimation or simulated spectroscopy, which rely on controlled unitaries as a subroutine, either using Hamiltonian simulation [28, 38–41, 43] or variational algorithms [16, 20]. We further analyse the noise robustness on spectral property estimation, including both coherent and incoherent noise. In the presence of device noise, the total running time maintains polynomial in inverse precision, showing advantages over existing approaches such as standard quantum phase estimation and Fourier transform of the time signals [23, 25, 26, 37]. We test the performance of the error mitigation strategy and the spectroscopic protocol by including the device and statistical noise in the numerical simulation. Finally, we investigate our method in cases of quantum spins, bosons, and fermions by numerics and simulation on IBM quantum devices. We show how transition energies and excitation spectra of spin-lattice models can be probed with IBM quantum devices with 13 qubits and over 350 two-qubit gates.

II. RESULTS

Motivation. The critical element in spectroscopy is the emergence of frequency excitations (and momentum excitations in translationally invariant systems) corresponding to the elementary excitations between eigenstates, which enables us to probe the transition energies as well as excitation spectra. Nevertheless, there are several constraints to conventional spectroscopy approaches, including (1) the perturbed system ρ is in an equilibrium state $[\rho, H] = 0$, (2) the perturbation is weak and the linear response theory holds. As there is no coherence of the initial state, (ρ is diagonal in the eigenbases $|n\rangle$ of the Hamiltonian, $\langle n|\rho|n'\rangle = \delta_{nn'}e^{-\beta E_n}$), we can only probe properties in the equilibrium phase.

The dynamical structure factor, which can be obtained from spectroscopy experiments, reflects the energy resonance between eigenstates $|n'\rangle$ and $|n\rangle$ and can be expressed as $S(\omega) = \sum_{n,n'} \rho^{nn} A_{n',n} \delta(E_{n'} - E_n - \omega)$ with $A_{n',n} = \langle n|\hat{O}_1^\dagger|n'\rangle \langle n'|\hat{O}_2|n\rangle$ and observables \hat{O}_1 and \hat{O}_2 (e.g. spin operators). The dynamical structure factor $S(\omega)$ is a Fourier transform of a two-point unequal-time correlation function $C(t) = \text{Tr}(\rho \hat{O}_1^\dagger(t) \hat{O}_2)$

in the Heisenberg picture on the equilibrium state ρ , $S(\omega) = \int_{-\infty}^{+\infty} C(t) e^{i\omega t} dt$. A straightforward way to detect the transition energy is by directly simulating the spectroscopy process, as studied in [16, 27, 28, 35]. However, it is less efficient since the time complexity for realising the spectral function $S(\omega)$ is large and an ancillary qubit is required for measuring $C(t)$ when using the Hadamard-test circuit. In addition, we need to prepare a thermal state ρ and can detect the equilibrium properties only. This raises the question of whether we can reduce the simulation time while maintaining simulation accuracy.

Framework. Here we develop a framework for estimating transition energies between the eigenstates of a quantum many-body system. Let us consider a quantum operation $\mathcal{G}(\rho, \omega) = \sum_{n,n' \geq 0} \rho^{n'n} |n'\rangle \langle n| p_\tau(E_{n'} - E_n - \omega)$, where $\rho^{n'n} := \langle n'|\rho|n\rangle$ and a function $p_\tau(\cdot)$ that selects the energy difference between eigenstates $|n'\rangle$ and $|n\rangle$ is introduced, for instance, the Gaussian function $p_\tau(\omega) = \exp(-\tau^2 \omega^2)$. With a properly selected observable \hat{O} , we can obtain the measurement outcome $G(\omega) = \text{Tr}[\mathcal{G}(\rho, \omega) \hat{O}]$ which can be expressed by

$$G(\omega) := \sum_{n,n' \geq 0} \Gamma_{n',n} p(\tau(E_{n'} - E_n - \omega)), \quad (1)$$

where $\Gamma_{n',n} := \rho^{n'n} \langle n|\hat{O}|n'\rangle$ represents the state-and-observable dependent coherence, yet is time-independent; $\Gamma_{n',n}$ can also be regarded a spectral weight associated with the initial state and observable. Here, we first arrange that $p_\tau(\omega) = p(\tau\omega)$, such that τ is coupled with ω . The quantity $G(\omega)$ contains the information on transition energies $\Delta_{n',n} := E_{n'} - E_n$. Specifically, given a proper $p(\cdot)$ and a large coherence $\Gamma_{n',n}$ between $|n'\rangle$ and $|n\rangle$, $G(\omega)$ takes its local maximum when ω approaches $\Delta_{n',n}$, and thus serves as a spectral detector. $G(\omega)$ characterises similar features as that of the dynamic structure factor, but its realisation will require fewer quantum resources than the dynamic structure factor.

A question is how to effectively implement the quantum operation and estimate $G(\omega)$ in Eq. (1). A natural idea is to effectively realise $G(\omega)$ by real-time dynamics, which is usually easy to implement on quantum simulators. To do so, we consider a Fourier transform of $G(\omega)$. Specifically, the dual form of p via its Fourier transform is given by $\tilde{g}(t) := \int_{-\infty}^{+\infty} p(\tau\omega) e^{i\tau\omega t} d(\tau\omega)$, and its inverse form $p(\tau\omega) = \frac{1}{2\pi} \int_{-\infty}^{+\infty} \tilde{g}(t) e^{-i\tau\omega t} dt$. Consider the normalised function $g(t) = |\tilde{g}(t)|/c$ with the normalisation factor $c := \int_{-\infty}^{+\infty} |\tilde{g}(t)| dt$ and phase $e^{i\theta t} := \tilde{g}(t)/|\tilde{g}(t)|$, and we have $g(t) = \frac{1}{c} \int_{-\infty}^{+\infty} p(\tau\omega) e^{-i\theta t} e^{i\tau\omega t} d(\tau\omega)$ and its dual form $p(\tau\omega) = \frac{c}{2\pi} \int_{-\infty}^{+\infty} g(t) e^{i\theta t} e^{-i\tau\omega t} dt$. Plugging the Fourier transform of p into Eq. (1), the spectral detector takes the form of

$$G(\omega) = \frac{c}{2\pi} \int_{-\infty}^{+\infty} G(\tau t) g(t) e^{i\theta t} e^{i\tau\omega t} dt \quad (2)$$

with $G(t) := \text{Tr}[\hat{O}\rho(t)]$ in the Schrödinger picture. Eq. (2)

indicates that we can first obtain $\text{Tr}[\hat{O}\rho(\tau t)]$ by measuring \hat{O} on the time-evolved state at time τt , and then use Eq. (2) to obtain $G(\omega)$. Since $g(t)$ is normalised and hence can be regarded as a probability distribution, a single-shot estimator of $\hat{G}(\omega)$ takes the form of

$$\hat{G}(\omega) = \frac{c}{2\pi} \delta(\tau t_i) e^{i\theta_{t_i}} e^{i\tau\omega t_i}, \quad (3)$$

where t_i is sampled from the distribution $g(t)$ which is τ -independent, and $\delta(\tau t_i)$ is an unbiased estimate of $\text{Tr}[\hat{O}(\tau t)\rho]$. One can verify that $\hat{G}(\omega)$ is an unbiased estimator of $G(\omega)$, $G(\omega) = \mathbb{E}\hat{G}(\omega)$, where the average is taken over the probability distribution $g(t)$. Here, we choose to treat $\tau\omega$ as a whole in Eq. (2) when performing the Fourier transform. As such, $g(\cdot)$ is a τ -independent probability distribution, and the total time length for evaluating $G(\omega)$ is τt , which is extended by a factor τ compared to original Fourier transform. An advantage of this treatment is that it enables a simple evaluation of the resource requirements using different functions p within a unified framework, rather than a case-by-case analysis. Alternatively, we can treat τ as a variable (in $p_\tau(\cdot)$) that is independent of ω , and hence will not be Fourier-transformed. These two ways are proven to be equivalent in Methods.

There are two necessary requirements for inferring the transition energy $\Delta_{n',n}$ using the spectral detector in Eq. (1): (1) a sufficiently large state-and-observable coherence $\Gamma_{n',n}$, and (2) a proper function $p(\omega)$ (or equivalently its dual form $g(t)$) that ensures that $\Delta_{n',n}$ can be distinguished from other transition energies. The coherence $\Gamma_{n',n}$ is time-independent yet dependent on the state and the chosen observable. In the following sections, we first discuss the selection of the initial state and observables in order to satisfy the first condition. We then show that by choosing the Gaussian function $p(\omega)$, our method only requires short-time dynamics to achieve high-precision energy estimation.

In a concurrent work [42], Yang *et al.* developed a similar method for evaluating the energy gap by introducing a so-called tuning parameter to increase the convergence rate, although the choice of the tuning parameter is not discussed and is fixed in numerics. Within our framework, the tuning parameter can be regarded as a separate parameter that is irrelevant to the Fourier transform.

Spectroscopic protocol. Now, we discuss the selection of the initial state and observables in several representative quantum systems such that $\Gamma_{n',n}$ is nonvanishing. Several works have discussed how to probe the excitation spectra by engineering the controllable quantum system [8, 24, 25, 44–48]. The basis of the spectroscopic protocols is that the initial state is populated by a superposition of low-lying excited states, which could be expressed as $|\psi_0\rangle = \sum_j a_j |j\rangle$ where $|j\rangle$ is an eigenstate of H . The initial state, generated by a global or local operation \hat{B} , could be formally expressed as $|\psi_0\rangle = b^{-\frac{1}{2}} \hat{B} |0\rangle$. Here $b := \langle \psi_0 | \hat{B}^\dagger \hat{B} | \psi_0 \rangle$ is the normalisation factor, and

$|0\rangle$ denotes the ground state of H . The observation in relation to the transition between the excited state and the ground state is $\langle n | \hat{O} | 0 \rangle = \sum_j a_j b^{\frac{1}{2}} \langle n | \hat{O} \hat{B}^{-1} | j \rangle$, and the state-and-observable coherence can be nonzero by choosing an appropriate \hat{B} .

In solid systems, translation invariance is usually conserved and the Hamiltonian satisfies $[H, \hat{\mathbf{P}}] = 0$, where $\hat{\mathbf{P}}$ is the total momentum operator. Each eigenstate $|n\rangle$ has a well-defined momentum of \mathbf{p}_n , $\hat{\mathbf{P}} |n\rangle = \mathbf{p}_n |n\rangle$. Suppose we choose the observable at position \mathbf{x} , $\hat{O}(\mathbf{x}) = e^{-i\hat{\mathbf{P}} \cdot \mathbf{x}} \hat{O} e^{i\hat{\mathbf{P}} \cdot \mathbf{x}}$ with $\hat{O} := \hat{O}(\mathbf{0})$. Taking a space Fourier transform of $G_x(\omega)$ in Eq. (1) with the observable $\hat{O}(\mathbf{x})$, $G_k(\omega) = \int d\mathbf{x} e^{-i\mathbf{k}\cdot\mathbf{x}} G_x(\omega)$, we have

$$G_k(\omega) = 2\pi \sum_{n,n'=0} \Gamma_{n',n} p(\tau(E_{n'} - E_n - \omega)) \delta(\mathbf{p}_{n'} - \mathbf{p}_n - \mathbf{k}), \quad (4)$$

when the system size reaches infinity and the translation invariance of the initial state is broken; for instance, the translation invariance of the state after applying a local operation to a single site is broken. The above equation indicates that translation invariance imposes selection rules of both energy and momentum for transition between eigenstates. This is the key element in spectroscopy detection, where elementary excitations between eigenstates emerge when the selection rules of energy and momentum are both satisfied.

Although in general a large coherence cannot be guaranteed (as this problem is quantumly hard; see Discussion), there are certain cases where we can manipulate the system to meet this requirement and allow for probing specific types of excitations. In a weakly coupled system, for instance, the particle excitations induced by perturbations are restricted to a manifold of single-particle excitations, as discussed in [25, 44]. In this limit, an excited state could be understood as a single particle (or quasiparticle) excitation above the ground state $|0\rangle$, $|n\rangle = \hat{\gamma}_{\mathbf{q}}^\dagger |0\rangle$, carrying momentum \mathbf{q} , where $\hat{\gamma}_{\mathbf{q}}^\dagger$ is the creation operator of a particle with momentum \mathbf{q} . Note that $\hat{\gamma}_{\mathbf{q}}^\dagger$ does not have to be the same creation operator in the Hamiltonian and could be either the creation operator of a particle or quasiparticle. The excitation generated from the ground state can be observed by choosing $\hat{O} = \sum_{\mathbf{p}} A_{\mathbf{p}} \hat{\gamma}_{\mathbf{p}} + A_{\mathbf{p}}^* \hat{\gamma}_{\mathbf{p}}^\dagger$, and we have $\langle 0 | \hat{O} | n \rangle = A_{\mathbf{q}} \delta_{\mathbf{q}\mathbf{p}}$. To probe the single particle excitation above the ground state with energy $E_n - E_0$, we may prepare the state containing a small perturbation with momentum \mathbf{q} as $|\psi_0\rangle \approx |0\rangle + \beta |n\rangle$ where β is a small constant (see [49] and Supplementary Section III). This choice of state and observable enables a nonzero observation as $\Gamma_{n,0} = \beta A_{\mathbf{q}}$, and the excitation spectrum can thus be observed.

We give some comments on more general cases. Let us consider the Hamiltonian which conserves either the particle or quasiparticle number. We denote the eigenstates of H as $|n\rangle$ and the vacuum state $|0\rangle$, and suppose the system has L modes (either in real space or momentum space). Any single-particle state $\hat{\gamma}_{\mathbf{p}}^\dagger |0\rangle$, which is generated by creating a particle at the \mathbf{p} th mode, could be

decomposed into the basis of $|n\rangle$, and the decomposition coefficient is denoted as $\langle n|\hat{\gamma}_{\mathbf{p}}^\dagger|0\rangle := c_{n,\mathbf{p}}$. Given that the quasiparticle picture holds, we can prepare the initial state $|\psi_0\rangle = \frac{1}{\sqrt{1+\beta^2}}(1 + \beta\hat{\gamma}_{\mathbf{p}}^\dagger)|0\rangle$. Then the initial state coherence is $\rho^{n0} = \beta\langle n|\hat{\gamma}_{\mathbf{p}}^\dagger|0\rangle/(1 + \beta^2) = \beta c_{n,\mathbf{p}}/(1 + \beta^2)$. The transition amplitude observed by the annihilation operator on the \mathbf{p}' th mode is $\langle 0|\hat{\gamma}_{\mathbf{p}'}|n\rangle = c_{\mathbf{p}',n}^*$. Therefore the coherence observed by \hat{O} is given by

$$\Gamma_{n,0} = \sum_{\mathbf{p}'} \frac{\beta A_{\mathbf{p}'}}{1 + \beta^2} c_{\mathbf{p}',n}^* c_{n,\mathbf{p}}. \quad (5)$$

A similar fashion can be used to probe the transition energy between the excited states $|n\rangle$ and $|n'\rangle$ with the same particle number. We can prepare the initial state by creating two particles as $|\psi_0\rangle = \frac{1}{1+\beta^2}(1 + \beta\hat{\gamma}_{\mathbf{p}}^\dagger)(1 + \beta\hat{\gamma}_{\mathbf{p}'}^\dagger)|0\rangle$, and choose the observable $\hat{O} = \sum_{\mathbf{p},\mathbf{p}'} A_{\mathbf{p},\mathbf{p}'} \hat{\gamma}_{\mathbf{p}}^\dagger \hat{\gamma}_{\mathbf{p}'}$ which conserves the particle number. More detailed derivations of the coherence $\Gamma_{n',n}$ can be found in Methods. Since the Hamiltonian can be engineered, we can specifically engineer quantum devices to detect the energy excitation spectra of various quantum systems. Typical transitions could be observed by preparing initial states consisting of the desired superposition (see Methods and Supplementary Information for discussions).

When the target quantum system's eigenstates can be labelled, we could track this label and detect the energy difference between these two states. This condition is satisfied when the quasiparticle picture holds. For example, in the case of Fermi liquids, the low-energy eigenstates are labelled by a set of quantum numbers $n_{\mathbf{p},\sigma} = 0, 1$ (i.e., the occupation numbers) [50], and we can ensure a nonzero coherence in the thermodynamic limit. This approach can thus be useful in detecting Fermi-liquid and some non-Fermi-liquid systems such as BCS types of systems. Another application of this spectroscopy approach is that we could detect if a system exhibits a non-Fermi-liquid feature and identify the transitions from a Fermi-liquid to a non-Fermi-liquid phase.

In addition to the above example, spectroscopy protocols have demonstrated that excitations can be effectively created in many quantum systems through numerical simulations [24, 25, 51–53] or analogue quantum simulations [8, 23, 44] in cases of the Bose-Hubbard model [23, 24], spin chains [8, 13, 44], and disordered systems [47]. It is worth mentioning how our method differs from these spectroscopy protocols. In the first place, the aim here is energy extraction instead of the experimental observables in spectroscopy experiments. In neutron spectroscopy experiments, for example, the externally injected neutrons act as a weak perturbation, which can probe the intrinsic properties of materials in the equilibrium state. In global or local quench spectroscopy, the eigenstates are assumed to be nearly unchanged after the quench, which is similar to that in spectroscopy experiments, although the state will be driven out of equilibrium. Our method does not put such con-

straints on the eigenstates and is applicable for probing more general quantum many-body systems given that the coherence associated with the excitation is nonvanishing. Moreover, quench spectroscopy is essentially limited to analogue simulations, and thus cannot be used to probe the unequal-time correlation function or systems without particle conservation. Our framework enables a direct extension to the probing of higher-order time correlation functions. For example, we can probe the nonlinear spectroscopic features [6, 54] of the target system by applying perturbations multiple times (at time t_i for different i) and obtaining the corresponding higher-order time correlation functions. The advantages over analogue quantum simulations are discussed in Supplementary Section III. Recently, Ref. [55] presents a way of simulating the correlation functions in a linear response framework. Regarding the simulation of the spectroscopic features, this could be regarded as a special case of our method when taking the filter operator to be an identity and the comparisons can be found in Supplementary Information.

Error analysis and resource requirement. We then discuss the computational complexity in transition energy estimation. In order to observe $\Delta_{n',n}$, the coherence $\Gamma_{n',n}$ associated with the transition is assumed to be nonvanishing, i.e. $\Gamma_{n',n}$ can be lower-bounded by a polynomial of the inverse of system size N as $\Gamma_{n',n} \geq \Omega(\text{Poly}(\frac{1}{N}))$. This condition can be satisfied in certain cases as discussed above. For instance, in the above particle-number conserved case, the initial state is populated by a collection of low-lying excited states, in which $\Gamma_{n,0}$ is nonvanishing while $\Gamma_{n,n'\geq 1}$ is of higher order. To simplify the discussion, we will sort $\Delta_{n',n}$ in ascending order hereafter, and denote the ordered transition energies as Δ_j and the spectral gap difference as $\gamma_j := \min(\Delta_{j+1} - \Delta_j, \Delta_j - \Delta_{j-1})$. It is worth noting that in the excitation spectrum analysis, the index j of the gap difference runs over the possible allowed excitations which should satisfy the momentum and coherence selection rules.

The objective is to estimate the transition energy Δ_j within an error ε , i.e., $|\hat{\Delta}_j - \Delta_j| \leq \varepsilon$. From now on, this is converted into an estimation problem. Intuitively, Δ_j can be determined by searching peaks of the absolute value of $G(\omega)$ in the frequency domain ω . To see this point, let us rewrite $G(\omega)$ as

$$G(\omega) = \Gamma_j p(\tau(\Delta_j - \omega)) + \sum_{i \neq j} \Gamma_i p(\tau(\Delta_i - \omega)). \quad (6)$$

Given a large τ , the first term will be dominant in $G(\omega)$, and thus $G(\omega)$ is close to the peak value Γ_j only if ω is close to Δ_j . In addition, in the vicinity of Δ_j , i.e. $\omega \in [a_L, a_R]$, we have $\partial^2 G(\omega)/\partial^2 \omega < 0$. The transition energy can thus be estimated by finding the peak of the estimate $\hat{G}(\omega)$ concerning finite measurement, i.e., $\hat{\Delta}_j = \text{argmax}_{\omega \in [a_L, a_R]} |\hat{G}(\omega)|$. The results established in spectral filter methods can be used to analyse the simu-

lation cost [26, 30, 38–40]. The total running time (maximal evolution time \times sampling numbers) in [38] or [30] is proven to reach the Heisenberg limit for eigenenergy estimation as $\tilde{\mathcal{O}}(\varepsilon^{-1})$. Note that it is sub-optimal concerning the maximal time complexity, which is a more important metric for implementation with near-term devices due to their short coherence time. We shall see that a relatively small τ of the order of $\log(\varepsilon^{-1})$ suffices to suppress contributions from the other transition and enables accurate estimation of Δ_j , as found in the eigenenergy estimation task [40].

We illustrate the proof idea in the following and refer to Methods for details. For $\tau = \mathcal{O}(\gamma_j^{-1} \log^{\frac{1}{2}}(\varepsilon^{-1}))$, one can show that (1) $|\hat{G}(\omega) - \Gamma_j| < c_1 \tau^2 \varepsilon^2$, $\forall |\omega - \Delta_j| \leq 0.5\varepsilon$; (2) $|\hat{G}(\omega) - \Gamma_j| > c_2 \tau^2 \varepsilon^2$, $\forall |\omega - \Delta_j| \in [\varepsilon, 0.1\gamma_j]$. Here, c_1 and c_2 are some constants that are irrelevant to τ and ε yet are dependent on Γ_j , and γ_j is the gap difference (see Lemma 1 in Methods). This indicates that the distance $d = |\Gamma_j - \hat{G}(\omega)|$ is modulated by the estimation error $|\omega - \Delta_j|$, and consequently, Δ_j can be distinguished from the other transitions when ω approaches Δ_j . It is assumed that Γ_j is nonvanishing, otherwise the peak will not appear. Given the theoretical guarantees, we first get an estimate of $G(\omega)$ by Eq. (3), and Δ_j is then determined by finding the peak of $\hat{G}(\omega)$ over frequency ω . Note that calculating $\hat{G}(\omega)$ as a function of ω is a task involving purely classical computing, and does not cost any quantum resources.

A remaining issue is the error from the finite cutoff when evaluating the integral in Eq. (2) with the integral range from $(-\infty, +\infty)$ to $[-T, +T]$. We highlight that our framework allows for a straightforward evaluation of the truncation error and the requirement for T . One can easily find that $T = \mathcal{O}(\log^{\frac{1}{2}}(\varepsilon^{-1}))$ suffices to guarantee the cutoff error below ε . Therefore, a finite cutoff only contributes to a logarithmic factor to the circuit complexity. The algorithmic complexity concerning a finite τ , a finite cutoff T for the integral and a finite number of measurements is shown below. Given nonvanishing Γ_j , to guarantee that the estimation $\hat{\Delta}_j$ is close to the true value Δ_j within error ε , we require the maximum time $\mathcal{O}(\gamma_j^{-1} \log(1/\varepsilon))$ and the number of measurements $\tilde{\mathcal{O}}(\varepsilon^{-4} \Gamma_j^{-2} \gamma_j^4)$. The rigorous description and the proof can be found in Methods.

It is worth noting that the energy excitation of a periodic system typically is a collective behaviour and the spectral weights are concentrated around the allowed excitations. This can be seen from Eq. (4) where the momentum selection rule restricts the allowed excitations to those that satisfy this condition. In addition, the coherence condition will impose restrictions on the possible excitations that can be probed by the initial state and the observable; for example, the selection of certain mode \mathbf{p} in Eq. (5) in cases where single-particle excitations are primarily concerned. This implies that in certain systems, the total number of allowed excitations may not grow exponentially with respect to the system size.

The key element in this protocol is the measurement of observable dynamics $G(t)$, which can be implemented using Trotterised product formulae which are ancilla-free. Here, we consider using an improved Trotter formula developed in [56], which can effectively eliminate the Trotter error without sacrificing the precision advantage or introducing any ancillary qubits. Suppose the Hamiltonian can be decomposed into Pauli bases as $H = \sum_{l=1}^L \alpha_l P_l$ with P_l being the Pauli operator and $\|\alpha\|_1 := \sum_l |\alpha_l|$. The gate complexity for running the time evolution is $\mathcal{O}((\|\alpha\|_1 t)^{1+o(1)} L \log(\varepsilon^{-1}))$, and the small overhead in the power depends on the order of the Trotter algorithm. The asymptotic scaling for lattice models with nearest-neighbour interactions is $\mathcal{O}((Nt)^{1+o(1)} \varepsilon^{-o(1)})$ with the system size N . In the situation where the evolution time is $t = \mathcal{O}(N\gamma_j^{-1})$, the gate complexity scales as $\mathcal{O}(N^{2+o(1)} \varepsilon^{-o(1)} \gamma_j^{-1})$. We will then numerically investigate the performance of the spectroscopic approach with an increasing system size.

A caveat is that some systems may become thermalised up to a certain time scale, for example, nonintegrable systems. In this situation, the initial state information is lost up to a certain time, and the microscopic feature of the system may not be resolvable by long-time evolution. We note that the spectral information is extracted from a relatively shorter time scale, which to some extent avoids this issue. It would be an interesting direction to discuss the appropriate time scale for resolving the target transitions.

Error effect in transition energy estimation. The preceding sections have discussed the algorithmic error due to finite simulation time and the uncertainty error. In this section, we will first discuss the algorithmic errors from Trotterisation or imperfect control of the Hamiltonian dynamics. Then, we will discuss errors due to imperfect quantum operations.

The effect of algorithmic errors from Trotterisation or imperfections of the Hamiltonian can be regarded as an additional term δH to the ideal Hamiltonian. For lattice models, the Trotter error conserves translation invariance and simply results in a shift to the energy spectrum. The new Hamiltonian also conserves translation invariance $\hat{\mathbf{P}}|\nu\rangle = \mathbf{p}_\nu|\nu\rangle$ where the eigenbasis of the new Hamiltonian is denoted as $|\nu\rangle$. The observable expectation is given by $\langle\nu|\hat{O}(\mathbf{x})|\nu\rangle = e^{i(\mathbf{p}_{\nu'} - \mathbf{p}_\nu)\cdot\mathbf{x}} \langle\nu|\hat{O}|\nu\rangle$. The momentum selection rule still holds, which imposes $\mathbf{k} = \mathbf{p}_{\nu'} - \mathbf{p}_\nu$ with the excitation between $|\nu'\rangle$ and $|\nu\rangle$ being connected by wavevector \mathbf{k} . However, noise will result in a deviation in transition energies. Up to the first-order perturbative expansion, $G(\omega)$ becomes

$$G(\omega) = \sum_{\nu', \nu} \Gamma_{\nu', \nu} p(\tau(\Delta_{\nu', \nu} - \omega)), \quad (7)$$

where $\Delta_{\nu', \nu} = \Delta_{n', n} + \langle n' | \delta H | n' \rangle - \langle n | \delta H | n \rangle$. The error results in a deviation of the resolved energy difference from the ideal one.

The first-order change in the ν th eigenstate is related to the unperturbed one by $|\nu\rangle = |n\rangle + \sum_{m \neq n} A_{mn} |m\rangle$ with $A_{mn} = \Delta_{nm}^{-1} \langle m | \delta H | n \rangle$. The coherence has a deviation from the unperturbed case,

$$\delta\Gamma_{\nu',\nu} = \alpha_{n'n} \langle n | \hat{O} | n' \rangle + \beta_{n'n} \rho^{n'n}, \quad (8)$$

where $\delta\Gamma_{\nu',\nu} = \Gamma_{\nu',\nu} - \Gamma_{n',n}$, and the coefficients are defined as $\alpha_{n'n} := \sum_m (A_{mn} \rho^{n',m} + A_{mn}^* \rho^{m,n})$ and $\beta_{n'n} := \sum_m (A_{mn} \langle n | \hat{O} | m \rangle + A_{mn}^* \langle m | \hat{O} | n' \rangle)$ which are related to the initial state and the observable, respectively. Compared to the unperturbed case, some eigenstates $|m\rangle$, which are absent in the original selection rule, also contribute to $\Gamma_{n',n}$ and hence change the spectral weight that can be observed by $G(\omega)$. In the presence of the disordered term which breaks the translation variance, the peaks of $G(\omega)$ will be broadened.

Resource requirement in the presence of device noise.

Finally, we analyse the effect of device noise, its mitigation and the resource requirement due to noise. We start with the discussion on errors in the process of implementation e^{-iHt} . Since this is a continuous process, a simple way to describe a physical noisy process is the following: the state remains unaffected with probability $\lambda\delta t$ while becomes a mixed state with probability $1 - \lambda\delta t$, with noise strength characterised by λ . This process is described by $\mathcal{E}_{\delta t}(\rho) = (1 - \lambda\delta t)\rho + \lambda\delta t\rho_{\text{mix}}$, where $\rho_{\text{mix}} = \frac{I}{2^N}$ is the maximally mixed state and I is the identity matrix. It is easy to see that the noise channel coupled with the unitary operator is only dependent on t and the effective action of such a noise channel is a global depolarising noise. To have an estimate of λ under the global noise model, we can fit the experimental results in a similar vein to randomised benchmarking, which could be robust against state preparation and measurement noise [57]. The expectation value of a Pauli operator is

$$\mathbb{E}\hat{O}_{\text{noisy}}(t) = \text{Tr}\left(\prod_{\delta t}^T (\mathcal{E}_{\delta t} \circ \mathcal{U}_{\delta t})(\rho_0)\right) = \Lambda(t)^{-1} \mathbb{E}\hat{O}_{\text{ideal}}(t) \quad (9)$$

with $\Lambda(t) = e^{\lambda t}$. This result indicates that under depolarising types of noise, the ideal expectation value can be obtained by multiplying the factor $\Lambda(t)$ to the noisy result. In some circumstances, the realistic circuit noise may be converted to a global white noise by Pauli twirling [57, 58] and as studied in Refs. [59, 60], shallow quantum circuits can scramble the noise into global white noise. We numerically verify that the global white noise ansatz could be used to approximate physical noise in certain circumstances, such as local depolarising noise, with simulation results shown in Methods.

For more general noise and its mitigation, when the total noise strength is bounded, we can still mitigate errors by probabilistic error cancellation [61–63], and the strategy is discussed in Supplementary Section II.1. Due to error mitigation, the variance of $G(\omega)$ will be amplified

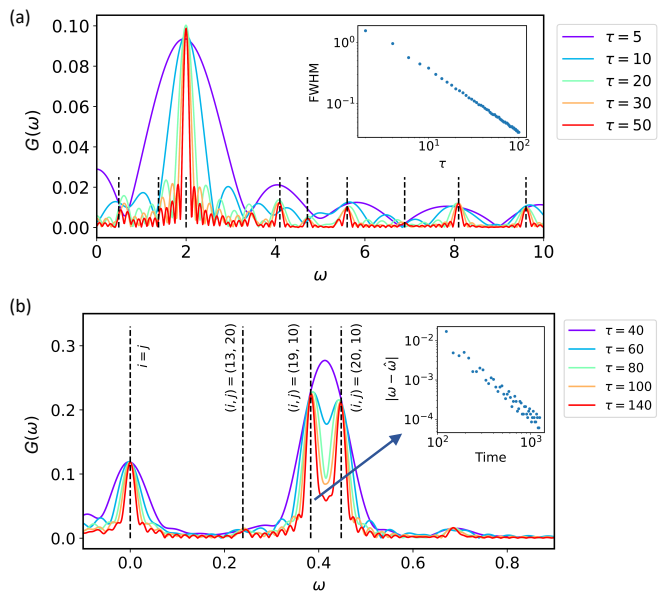


FIG. 1. **Transition energy spectra search of the Heisenberg model and the LiH molecule.** **a** The 7-site Heisenberg model. The state is first initialised in a product state $|+\rangle^{\otimes N}$, and then a rotation is applied to the central qubit, which takes the form of $\hat{\sigma}_3^x |+\rangle^{\otimes N}$, where the qubit numbering starts from zero in this work. The dashed vertical lines show the ideal transition energies whose coherence $\Gamma_{i,j}$ is above a certain threshold, which are calculated by exact diagonalisation (ED). Inset: FWHM dependence on varying τ . The cutoff is chosen as $T_{\text{cut}} = 1$. **b** The excitation spectrum for LiH. The initial state is prepared as a Hartree-Fock state. The vertical lines show the ideal transition energies $\Delta_{i,j}$ calculated by ED. Inset: Estimation error for the dominant transition energy indicated by the arrow with varying total time.

by $\max_t \Lambda(t)$. In the presence of noise, the number of samples required by our method maintains polynomial in inverse precision $\mathcal{O}(\text{poly}(1/\epsilon))$. On the other hand, other methods based on the Fourier transform of the time signals or quantum phase estimation will require an amplified number of samples $\mathcal{O}(\exp(1/\epsilon))$. Our method thus shows certain advantages over the existing methods when considering device noise. The simulation results incorporating noise and noise mitigation are shown in Methods. More detailed discussions on error mitigation and resource requirements can be found in Supplementary Section II.

Numerical studies and experimental demonstration on IBM quantum devices. We investigate the performance of our method for probing the energy excitation spectrum of quantum many-body systems by numerical simulation and experimental demonstration on IBMQ devices. We consider a local perturbation applied to the initial product state, which generates a branch of low-lying excitations of the system. Then the system is evolved under unitaries $U = e^{-iHt_i}$ with different times t_i drawn from the Gaussian distribution $g(t)$, followed by

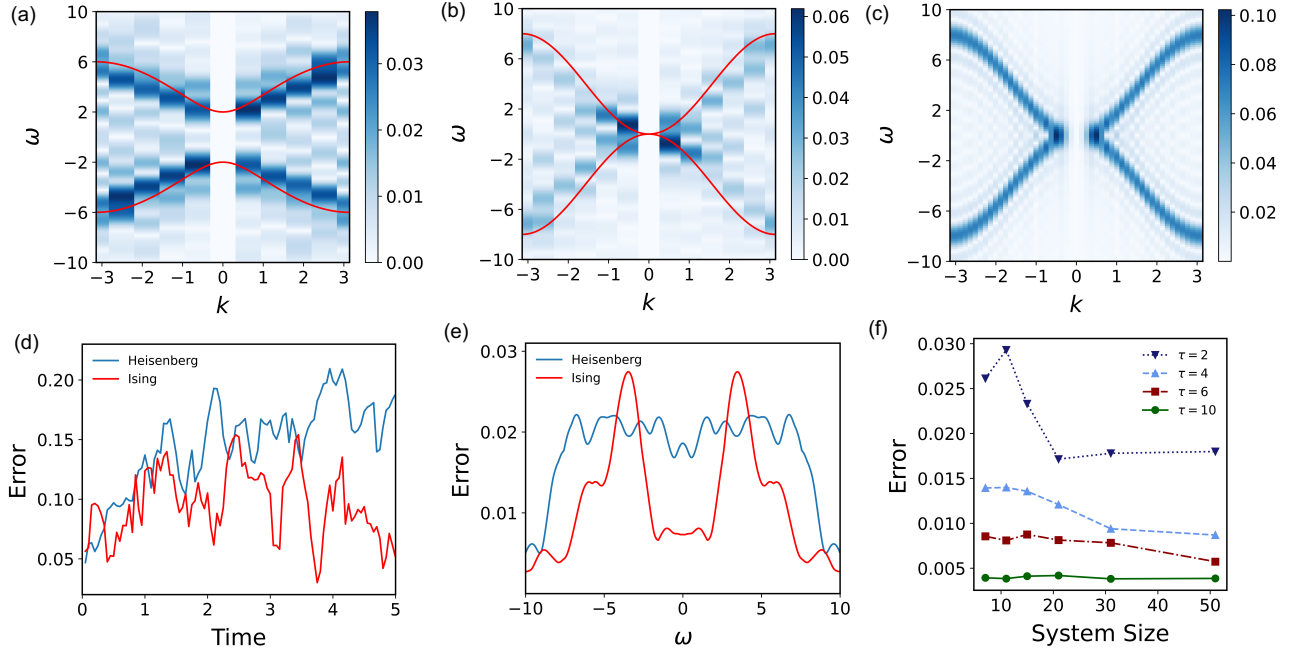


FIG. 2. **The energy dispersions of 1D lattice models through the demonstration on the IBM quantum devices (a,b,d,e) and tensor-network simulation (c,f).** **a** The excitation spectra $G(\omega)$ of an 11-site Ising model. **b** The excitation spectra of a 13-site Heisenberg model. The results are obtained from measurements on IBMQ devices. The red lines in **a** and **b** represent the energy dispersions of infinite long spin chains obtained by analytic calculations. The intensities at $\mathbf{k} = 0$ have been removed. **c** The energy dispersion for the 1D Heisenberg chain of length $N = 51$ with $h_z = 0$ and $J = 1$. The total time evolution is set as $T_{\text{tot}} = \tau = 5$. **d** Experimental simulation error for the measurement results of $\sum_i \langle \hat{\sigma}_i^y(t) \rangle / N$ under real-time evolution conducted on IBMQ devices, which is compared to results using noiseless Trotter formulae for both the Ising Hamiltonian (red line) and the Heisenberg Hamiltonian (blue line). **e** Experimental simulation error for the measurement results $G(\omega)$ from IBMQ experiments in the frequency domain averaged over different momenta. The results in **d** and **e** are compared to those using noiseless Trotter formulae. The maximal time length is $T_{\text{tot}} = 5$. **f** Scalability analysis for the gapless Heisenberg chain. The numerical simulation results for different values of τ are compared with the approximately ideal case in which $\tau \rightarrow \infty$. The figure shows the maximum error of the intensity $G(\omega)$ in the momentum space for different time scales τ and system sizes. The error is calculated as $\max_k |G_{k,\tau}(\omega) - G_{k,\tau \rightarrow \infty}(\omega)|$ where the averaging has been taken over ω .

quantum measurement.

We first demonstrate how transition energies can be estimated. Let us consider a one-dimensional (1D) Heisenberg model with an external field

$$H = J \sum_i (\hat{\sigma}_i^x \hat{\sigma}_{i+1}^x + \hat{\sigma}_i^y \hat{\sigma}_{i+1}^y + \hat{\sigma}_i^z \hat{\sigma}_{i+1}^z) + h_z \sum_i \hat{\sigma}_i^z, \quad (10)$$

with the periodic boundary condition, where $\hat{\sigma}_i^\alpha$ is the Pauli operator along the α axis acting on the site i , $J = -1$ is the ferromagnetic coupling strength, and h_z is the external magnetic field. To break the ground state degeneracy and make more excitations emerge, a small field $h_z = 10^{-2}J$ aligned in the z -direction is applied. The observable is chosen as $\hat{\sigma}_i^y$ on each site, which reverses the quench operation. The transition energy spectrum of the Heisenberg model is shown in Fig. 1(a). The peaks become sharper and thus distinguishable with increasing time. We find that the transition energies for the Heisenberg model are estimated very accurately because the dominant transition is distinguishable from the other ones. Fig. 1 inset shows the full width of the peak

at half maximum (FWHM) with increasing time.

We then show results for estimating transition energies for molecular systems, taking LiH as an example. The molecular Hamiltonian of LiH at the bond length $r = 5.0\text{\AA}$ is encoded into six qubits by Jordan-Wigner mapping. The observable is chosen as a particle-conserving operator $\hat{c}_0^\dagger \hat{c}_1 + \hat{c}_0 \hat{c}_1^\dagger$ with fermionic (creation) annihilation operator \hat{c} (\hat{c}^\dagger), which considers the transitions between low-lying excited states, in order to make $\langle n | \hat{O} | n' \rangle$ non-vanishing. The transition states are marked alongside the corresponding energy resonance in Fig. 1(b). In molecular systems, the excited states of molecular systems are often closely spaced, resulting in interference between different transitions. As a result, the visible peak appears as an addition of different peaks, making it difficult to locate the true transitions from the peak. However, as time increases, the peaks become sharper and more peaks appear, which allows for the distinction of the true transition. The inset of Fig. 1(b) shows the estimation error with increasing time for the dominant transition. It is worth noting the initial state remains a low-lying excita-

tion above the ground state, and the first few low-lying excited states are degenerate. As molecules become more complex, it is anticipated that more near-degenerate low-lying states will emerge, leading to an increase in peak interference and hence a more intricate spectrum. To distinguish small, adjacent peaks, we need to increase the evolution time. The results in Fig. 1 show how transition energies can be estimated and how the simulation accuracy can be improved by increasing the simulation time. The evolution of peaks of other molecules with varying time and their spectral weights can be found in Supplementary Section IV.

Next, we show how the excitation spectra of lattice models can be probed with the IBM Kolkata quantum device. We consider the 1D Ising model $H = \sum_i \hat{\sigma}_i^z \hat{\sigma}_{i+1}^z + 2 \sum_i \hat{\sigma}_i^x$ with nearest-neighbour interaction. The ground state is close to the product state when the external field is large, and thus we consider the excitation being generated by a local perturbation. The initial state is prepared as $|\psi_0\rangle = R_y^i(\frac{\pi}{2})|+\rangle^{\otimes N}$ with the single-qubit rotation operation acting on the central site i . Similarly, we demonstrate the simulation of the 1D Heisenberg model in Eq. (10) with $h_z = 0$ and $J = 1$. The time evolution is simulated using Trotter formulae with an even-odd order pairing method such that the Trotter error is reduced. More details about the circuit compilation can be found in Methods. The excitation spectra of the Ising model and the Heisenberg model are shown in Fig. 2(a,b), respectively. The energy dispersions for both models are in good agreement with the analytic results for infinitely long spin chains. The experimental simulation errors for the observable dynamics and energy excitations are shown in Fig. 2(d,e), respectively. The simulation on the Kolkata device involves over 350 CNOT gates, but the simulation error is maintained at an acceptable level, which indicates the robustness of our method.

The maximum system size is restricted by the large noise and the available size of the hardware. To further show the performance of our method for a relatively large system, we numerically test our method with an increasing system size using tensor network methods. We show the simulation error with different system sizes up to 51 qubits in Fig. 2(f). The error is decreased by increasing τ , and it is not increased with increasing system size. In Fig. 2(c), we show the excitation spectra of the 51-site Heisenberg model for comparison with the experimental result in Fig. 2(b). We refer to Supplementary Section IV for more results of excitation spectra simulation of the 2D Heisenberg model, the Bose-Hubbard and the Fermi-Hubbard model. Note that the examples studied here are classically simulable by tensor networks since the central aim is to test the performance of our method for known systems under different conditions. We do not attempt to prove a quantum advantage over classical computing or show its generality for solving arbitrary quantum systems. Instead, we aim to show how the spectroscopic properties of many-body systems can be probed using ei-

ther analogue or digital quantum simulators as a proof of concept.

We remark that simulating general gapless systems is a widely believed challenge, which poses great challenges to most existing algorithms, such as phase estimation and quantum singular value transformation [64]. The difficulty is that the energies are highly degenerate such that energy is not sufficient to distinguish these states. By introducing other conjugate variables, we could label the states with both the energy and the auxiliary characters (e.g. energy and momentum (E, k)) such that the degenerated states can be distinguished. Therefore, this strategy may be useful for analysing gapless systems with certain symmetry conservation, like translation invariance. Although we only test for simple and specific examples in this work, the results might shed light on the resolution of energy spectra of other gapless systems. The spectroscopic method and the examples examined here could potentially stimulate further discussions on estimating the properties of gapless systems.

III. DISCUSSION

In this work, we introduce a spectroscopic method for probing transition energies and excitation spectra of quantum many-body systems. The framework presented in this work establishes a connection between spectroscopic techniques and quantum simulation, and thus enables mutual benefits and advancements in both fields. The key element is the realisation of frequency resonance, and one can detect systems with certain symmetries by introducing additional momentum resonance. Our method requires the implementation of short-time dynamics only with the time length logarithmic in precision, and could be experiment-friendly for the current generation of quantum simulators. Advanced measurement algorithms [36, 65] (e.g. classical shadows [36]) can be directly employed to reduce the measurement complexity in measuring observables within this framework (see Methods for details).

We numerically test the scalability of the spectroscopic method for lattice models including both gapped and gapless cases. The simulation results obtained for gapless systems with translation invariance imply that our method may be useful for analysing similar systems with certain symmetry conservation, and we leave it to future work. We note that when the ground-state energy is known, finding the transition energy between the excited state $|n\rangle$ and the ground state $|0\rangle$ is equivalent to the problem of finding the eigenenergy of a quantum system. Therefore, resolving the transition energy could be quantumly hard. Our method is efficient when the state and observable dependent coherence is nonvanishing which could be satisfied in several quantum systems with the conservation of particle numbers. Though this in general does not hold, we tested the coherence for molecules and lattice models. On the other hand, we remark that

although we do not expect that our method can resolve the transition energy for general systems, the spectroscopic protocol can find applications in simulating the energy excitation spectrum; in this task the excitation is a collective behaviour and hence we do not necessarily require resolving a specific energy transition. In addition, the simulated spectroscopic features could be useful for identifying the transition from a Fermi-liquid to a non-Fermi-liquid phase and pinpointing the breakdown of where the quasiparticle picture no longer holds.

The simulation result suggests that the spectral properties of several quantum many-body systems can be estimated with high accuracy, even with increasing system sizes for lattice Hamiltonians considered in this work and when statistical and device noise are present. We also demonstrated how our method can be applied to probe the excitation spectra of spin Hamiltonians on IBM quantum devices. These results indicate that our approach could serve as a quantum computing solution complementary to high-intensity scattering facilities. For example, it could be useful in stimulating new quantum computing-based methods for resolving complex many-body systems with different conditions, such as various materials-dependent conditions (e.g. doping levels) and environmental conditions (e.g. pressure and temperature).

METHODS

Equivalence of the two formalisms. The function $p(\cdot)$ plays a role as a spectral detector that can filter $\Delta_{n'n}$ out of the other transition energies. In this work, we focus on the Gaussian function since the truncation error is small. Other functions can be chosen, and the resource requirement can be easily analysed under our framework.

If τ is introduced as a separate parameter that is irrelevant to the Fourier transform, it is straightforward to have $\tilde{g}_\tau(t) := \int_{-\infty}^{+\infty} p_\tau(\omega) e^{i\omega t} d\omega$ and $p_\tau(\omega) = \int_{-\infty}^{+\infty} \tilde{g}_\tau(t) e^{-i\omega t} dt$. One can check that $\tilde{g}_\tau(t) = \frac{1}{\tau} \tilde{g}(\frac{t}{\tau})$, where \tilde{g} was defined in the main text. We have

$$p_\tau(\omega) = \frac{c(\tau)}{2\pi} \int_{-\infty}^{+\infty} \text{Pr}(t, \tau) e^{i\theta t} e^{-i\omega t} dt \quad (11)$$

where $c(\tau) := \int_{-\infty}^{+\infty} |\tilde{g}_\tau(t)| dt = c$ and $\text{Pr}(t, \tau) := |\tilde{g}_\tau(t)|/c(\tau)$. On the other hand, we can arrange that τ is coupled with ω in the Fourier transform, which is the way introduced in the main text. One can check that Eq. (11) is equivalent to $p(\tau\omega)$ defined in the main text, and thus the two formalisms are equivalent. One important point to highlight is that the function $g(t)$ is τ -independent and is normalised. That means we can easily analyse and compare different methods in a unified framework, rather than a case-by-case analysis. Therefore, the method presented in the main text facilitates a straightforward evaluation of the resource requirement.

More detailed derivations can be found in Supplementary Section I.

We remark that our approach is capable of estimating the energy differences between energy eigenstates by identifying the peaks in the excitation spectrum. However, applying the spectral filter will alter the width of the peak, in contrast to conventional spectroscopic techniques. Therefore, properties in relation to the peak width, such as the lifetime of quasiparticles, cannot be determined. In addition, the introduction of a filter function will alter the width of the peak. Therefore, we cannot distinguish whether the broadening of the peak is caused by a finite evolution time or a continuum, because both can lead to a broadening of the peak.

Analysis of the algorithmic error and resource requirements. In this section, we first discuss the coherence in particle-conserved systems. Then, we analyse the estimation error of the transition energies under a finite imaginary time τ , a finite cutoff T when evaluating the integral, and a finite number of measurements N_s . Based on the error analysis, we estimate the resource requirement for transition energy estimation.

The observable is assumed to have a bounded norm $\|\hat{O}\| \leq 1$; for instance, the observable can be chosen as a tensor product of single-qubit Pauli operators. Consequently, we have $|\text{Tr}(\hat{O}\rho)| \leq 1$ and $\max_j \Gamma_j \leq 1$. As $\text{Tr}(\hat{O}\rho) = \sum_{n,n'} \rho^{n'n} \langle n|\hat{O}|n'\rangle$, the sum of the spectral weight has an upper bound $\sum_{n,n'} \Gamma_{n'n} \leq 1$. We will discuss the condition for ensuring a nonzero coherence in particle-conserved systems in the following.

In the main text, we showed that for certain many-body systems, by measuring the (quasi)particle annihilation and creation operator $\hat{O} = \sum_{\mathbf{p}'} A_{\mathbf{p}'} \hat{\gamma}_{\mathbf{p}'}^\dagger + A_{\mathbf{p}}^* \hat{\gamma}_{\mathbf{p}}$, we can observe the transitions (since $\Gamma_{n,0} \neq 0$). In a special case, for Bose-Hubbard models, as has been demonstrated experimentally for the hard-core boson cases in [23], we may consider the measurement of \hat{a}_r which is the original bosonic annihilation operator on the r th site in this context. This is a special case of our choice. Since the $\hat{a}_r = \hat{x}_r + i\hat{p}_r$ where \hat{x}_r and \hat{p}_r are the canonical coordinates for the r th mode, the measurement of $\langle \hat{a}_r \rangle$ could be realised by measuring in the single-mode canonical coordinates and then post-processing the measurement outcomes.

To probe $\Gamma_{n',n}$, we could choose to initialise the state by creating two particles above the vacuum state as $|\psi_0\rangle = \frac{1}{1+\beta^2} (1 + \beta\hat{\gamma}_{\mathbf{p}}^\dagger)(1 + \beta\hat{\gamma}_{\mathbf{p}'}^\dagger)|0\rangle$. Again, we can decompose the single-particle state $\hat{\gamma}_{\mathbf{p}}^\dagger|0\rangle$ with momentum \mathbf{p} into the single-particle eigenbasis of $|n\rangle$, and we denote the expansion coefficient $\langle n|\hat{\gamma}_{\mathbf{p}}^\dagger|0\rangle := c_{n,\mathbf{p}}$ with the normalisation condition $\sum_n |c_{n,\mathbf{p}}|^2 = 1$. We could find that in the case where the number of possible excitations grows polynomially with respect to the system size the coefficient will be nonvanishing. Similarly, for the two-particle state, we can decompose it into the two-particle eigenbasis of $|n^{(2)}\rangle$, and we denote the expansion coefficient

cient $\langle n^{(2)} | \hat{\gamma}_{\mathbf{p}}^\dagger \hat{\gamma}_{\mathbf{p}'}^\dagger | 0 \rangle := c_{n, \mathbf{p}\mathbf{p}'}^{(2)}$.

If we simply wish to observe the transitions in the single-particle manifolds, then for the observable $\hat{O} = \sum_{\mathbf{q}, \mathbf{q}'} A_{\mathbf{q}, \mathbf{q}'} \hat{\gamma}_{\mathbf{q}}^\dagger \hat{\gamma}_{\mathbf{q}'}$, the transition amplitude between single-particle eigenstate $|n\rangle$ and $|n'\rangle$ may be approximated by $\langle n | \hat{O} | n' \rangle = \sum_{\mathbf{q}, \mathbf{q}'} A_{\mathbf{q}, \mathbf{q}'} c_{n, \mathbf{q}} c_{\mathbf{q}', n'}^*$. Here we have put a strong assumption that the space of eigenstates with different particle numbers is orthogonal, specifically $\langle n | \hat{\gamma}_{\mathbf{q}}^\dagger | m \rangle = 0$ for $m \neq 0$. We conjecture that this condition holds when the quasiparticle number is well-defined. The transitions in the many-particle manifolds are more complicated; we may deliberately choose the observable to infer the transition energy. In our case, the initial state coherence is

$$\rho^{n', n} = \frac{\beta^2}{(1 + \beta^2)^2} (c_{n', \mathbf{p}'} + c_{n', \mathbf{p}}) (c_{\mathbf{p}', n}^* + c_{\mathbf{p}, n}^*).$$

To sum up, the coherence is given by

$$\Gamma_{n', n} = \sum_{\mathbf{q}, \mathbf{q}'} \frac{\beta^2 A_{\mathbf{q}, \mathbf{q}'} c_{n, \mathbf{q}} c_{\mathbf{q}', n'}^*}{(1 + \beta^2)^2} (c_{n', \mathbf{p}'} + c_{n', \mathbf{p}}) (c_{\mathbf{p}', n}^* + c_{\mathbf{p}, n}^*). \quad (12)$$

We give a few comments on the coherence in many-body quantum systems. As discussed in the main text, systems that host quasiparticles satisfy the condition for a nonvanishing coherence. For Fermi liquid, the low-energy eigenstates are labelled by a set of quantum numbers $n_{k, \sigma} = 0, 1$ (the occupation numbers) and the introduction of interactions will not let the quasiparticle decay into multiple other quasiparticles [50]. The one quasiparticle state has a finite overlap with the state where a bare particle carrying the same quantum numbers is added. More concretely, the overlap between the quasiparticle state $|\psi_k\rangle$ carrying momentum k and the ground state $|\psi_0\rangle$ excited by $\hat{c}_{k, \sigma}^\dagger$, $|\langle \psi_k | \hat{c}_{k, \sigma}^\dagger | \psi_0 \rangle|^2$, is not zero in the thermodynamic limit for k near the Fermi surface. Note that the overlap is between 0 and 1 because the quasiparticle state $|\psi_k\rangle$ is a superposition of all states with momentum k . This property gives a guarantee for the nonzero coherence. The non-metallic states such as anti-ferromagnetic states are generated due to interactions between electrons and can be understood from this Fermi liquid theory [50]. Nevertheless, it is worth noting that finding the occupancy of the original orbitals in the interacting eigenstate $|n'\rangle$, $n_{\text{occ}}(k, \sigma) = \langle n' | \hat{c}_{k, \sigma}^\dagger \hat{c}_{k, \sigma} | n' \rangle$ is still a computationally hard task. The simulated spectroscopic features can thus be useful for understanding certain behaviours of many-body systems.

Although our method relies on the coherence between the target eigenstates, it could be useful in identifying certain spectroscopic features of the target system. For example, in the case of non-Fermi liquid, the lifetime of quasiparticles is short and its spectrum is expected to be blurred. This blurred spectroscopic feature indicates the beginning of non-Fermi-liquid behaviour. Understanding this blurred behaviour in nature is an interesting question, and our approach can help reveal it. The simu-

lated spectroscopic features could be useful for identifying the transition from a Fermi liquid to a non-Fermi-liquid phase and pinpointing the breakdown of where Fermi liquid theory no longer holds.

Below, we will assume $\Gamma_{n', n}$ is nonzero and give the circuit complexity dependence on $\Gamma_{n', n}$. Recall that the spectral detector takes the form of

$$G(\omega) := \sum_{n, n' \geq 0} \Gamma_{n', n} p(\tau(E_{n'} - E_n - \omega)), \quad (13)$$

which can be simplified as $G(\omega) = 2 \sum_{n < n'} \Re(\Gamma_{n', n}) p(\tau(E_{n'} - E_n - \omega))$. For simplicity, we sort $\Delta_{n', n}$ in ascending order and denote ordered energies as Δ_i and the associated coherence is denoted as $\Gamma_i \leftrightarrow 2\Re(\Gamma_{n', n}) \in \mathbb{R}$. The spectral detector can now be expressed as $G(\omega) = \sum_i \Gamma_i p(\tau(\Delta_i - \omega))$. Then, the original problem is converted to a standard energy estimation problem as stated and studied in [38, 40].

Suppose we aim to estimate Δ_j with a nonvanishing Γ_j . Without loss of generality, we assume $\Gamma_j > 0$ in the following discussion, such that $G(\omega)$ is positive when ω approaches Δ_j (given a large Γ_j). Similar results can be obtained in the case of negative Γ_j . Intuitively, the spectral information can be inferred by looking at the peak of the intensity of $|G(\omega)|$. This is guaranteed by the following lemma.

Lemma 1. *When $\tau = \frac{1}{0.9\gamma} \sqrt{\ln\left(\frac{20}{\varepsilon^2 \Gamma_j}\right)}$ and $\varepsilon \leq 0.2\gamma$, the two inequalities hold:*

$$\Gamma_j - G(\omega) \leq 0.3\tau^2 \varepsilon^2 \Gamma_j, \forall |\omega - \Delta_j| \leq 0.5\varepsilon \quad (14)$$

and

$$\Gamma_j - G(\omega) \geq 0.8\tau^2 \varepsilon^2 \Gamma_j, \forall |\omega - \Delta_j| \in (\varepsilon, 0.1\gamma) \quad (15)$$

The above lemma guarantees that the distance $d = |\Gamma_j - \hat{G}(\omega)|$ is modulated by the estimation error $|\omega - \Delta_j|$. Therefore, Δ_j can be distinguished from the other transitions when ω approaches Δ_j . The next step is to analyse the quantum resources required to have a good estimation of $\hat{G}(\omega)$.

When evaluating the integral in Eq. (3) in the main text, we set a finite cutoff for the integral range from $[\infty, \infty]$ to $[-T, T]$ in practice. The truncated detector of $\hat{G}(\omega)$ is defined as

$$G^{(T)}(\omega) = \int_{-T}^T G(\tau t) g(t) e^{i\theta t} e^{i\tau\omega t} dt. \quad (16)$$

If a Gaussian operation is used, it is easy to check that the truncation error has an upper bound

$$|G^{(T)}(\omega) - G(\omega)| \leq 2 \int_T^\infty g(t) dt = \text{erfc}(T/2) \leq \exp(-T^2/4) \quad (17)$$

which has been discussed in prior work [38, 40]. Therefore, the truncation error can be bounded by

$$|G^{(T)}(\omega) - G(\omega)| \leq \varepsilon_T, \forall \omega \in \mathbb{R} \quad (18)$$

when the cutoff time $T \geq 2\sqrt{\ln(1/\varepsilon_T)}$.

In the following, we consider the error due to a finite number of measurements. A single-shot estimator of $G^{(T)}(\omega)$ takes the form of

$$\hat{G}_i^{(T)}(\omega) = \begin{cases} \hat{\omega}(\tau t_i) e^{i\theta_{t_i}} e^{i\tau\omega t_i}, & |t_i| \leq T \\ 0, & |t_i| > T \end{cases} \quad (19)$$

where the time length t_i is drawn from the probability distribution $g(t)$, which is τ -independent, and $\hat{\omega}(\tau t_i)$ is an unbiased estimate of $\text{Tr}[\hat{O}(\tau t)\rho]$. We can estimate $G(\omega)$ by

$$\hat{G}(\omega) = \frac{1}{N_s} \sum_{i=1}^{N_s} \hat{G}_i^{(T)}(\omega), \quad (20)$$

where N_s is the total number of samples. It is worth noting at this juncture that both $\text{Tr}[\hat{O}(\tau t)\rho]$ and $G(\omega)$ are real numbers, in contrast to the cases in eigenenergy estimation where the expectation values are complex numbers.

The transition energy is estimated by

$$\hat{\Delta}_j = \text{argmax}_{\omega \in [\Delta_j - \gamma/2, \Delta_j + \gamma/2]} \hat{G}^{(T)}(\omega). \quad (21)$$

Note that it is assumed that $\Gamma_j > 0$. The result is summarised as follows.

Proposition 1. *To guarantee that an estimation $\hat{\Delta}_j$ of the transition energy Δ_j is close to the true value within an error ε , with a failure probability δ , we require that the maximum time is $\mathcal{O}(\gamma^{-1} \log(1/\varepsilon))$ and the number of measurements $\tilde{\mathcal{O}}(\varepsilon^{-4} \Gamma_j^{-2} \gamma^3 \log(1/\delta))$, where γ is a chosen lower bound of the gap difference $\gamma \leq \min\{\Delta_{j+1} - \Delta_j, \Delta_j - \Delta_{j-1}\}$ where j runs over the allowed excitations restricted by the energy and momentum selection rule.*

In this work we use the $\tilde{\mathcal{O}}$ notation where the polylogarithmic dependence is hidden. Proposition 1 indicates that the maximum circuit depth is logarithmic in precision and the total running time scales as $\tilde{\mathcal{O}}(\varepsilon^{-4})$, in contrast to the result established in [38] or [30] which is $\tilde{\mathcal{O}}(\varepsilon^{-1})$. The above result is guaranteed by Lemma 2 in Supplementary Information, which shows that the maximum time required is $t = \tau \times T = \mathcal{O}(\gamma^{-1} \log(\varepsilon^{-1}))$ and $N_s = \tilde{\mathcal{O}}(\varepsilon^{-4} \gamma^4 \Gamma_j^{-2} \log(\delta^{-1}))$. The total running time scales as $\tau \times T \times N_s = \tilde{\mathcal{O}}(\varepsilon^{-4} \gamma^3 \log(\varepsilon^{-1}) \log(\delta^{-1}))$. Proposition 1 naturally flows from the above analysis. We leave the proof for Lemma 1 and Lemma 2 to Supplementary Section I.

Complexity for measuring multiple observables. In the above analysis, we assume that $\|\hat{O}\| \leq 1$. It is easy to find that our method only requires measurement of $\langle \psi(t) | \hat{O} | \psi(t) \rangle$ and thus any kind of measurement scheme is directly applicable. Therefore, multiple low-support observables can be estimated in an efficient way. Suppose

there are N_o low-support observables to be measured and the conditions in Proposition 1 are satisfied. By employing classical shadow methods developed in [36], the total time complexity is $\mathcal{O}(\gamma^3 \varepsilon^{-4} \log(1/\varepsilon) \log(N_o))$, which is only amplified by a logarithmic factor compared to single observable estimation. Note that the measurement complexity scales exponentially with respect to the locality of the observables m as $\mathcal{O}(3^m)$. Advanced measurement algorithms can be directly employed within our framework, such as Pauli grouping methods [36, 65], whose efficiency in measuring qubit-wise compatible observables has been verified for various examples.

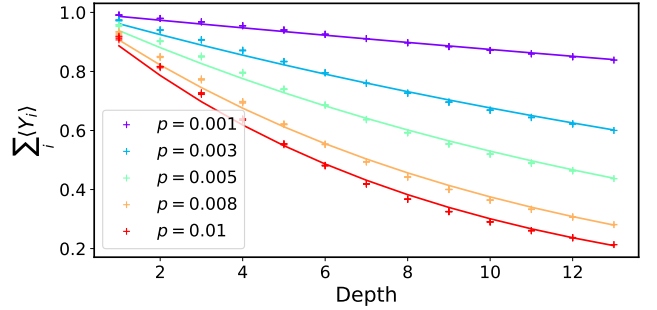


FIG. 3. **Fitting for the circuit evolution with local depolarising noise.** Numerical results of the circuit UU^\dagger implementation of noisy spectroscopy protocol for simulating the 7-site Ising model ($h_x = 2$ and $h_z = 0.1$) with different noise strength p . The depth refers to the repetition numbers. The solid lines represent the exponential fit for every p . All the regressions have a relative predictive power $R^2 = 0.99$.

Recently Chan et al. proposed to extract eigenenergy differences by post-processing classical shadows of time-evolved states [26]. The quantum resources and the signal-to-noise ratio were analysed. Since the extraction of eigenenergy differences is based on the post-processing of many time-evolved states, the low measurement cost is essential for their method. In this work, we show that for several quantum many-body systems, the observables are chosen with clear physical intuitions, which, to some extent, avoids the necessity of measuring many observables.

Numerical simulation based on tensor networks. For the numerical simulation conducted in this work, the time evolution e^{-iHt} is simulated using a time-dependent variational principle (TDVP) algorithm based on the representation by matrix product states (MPS). The density matrix renormalisation group (DMRG) method is used to initialise the system into the ground state of the system before applying quench. The following shows a few examples of excitation spectra simulation. In Supplementary Section IV, we show simulations of both the Bose-Hubbard and Fermi-Hubbard models. The Hamiltonian for both bosons (BH) and fermions (FH) can be

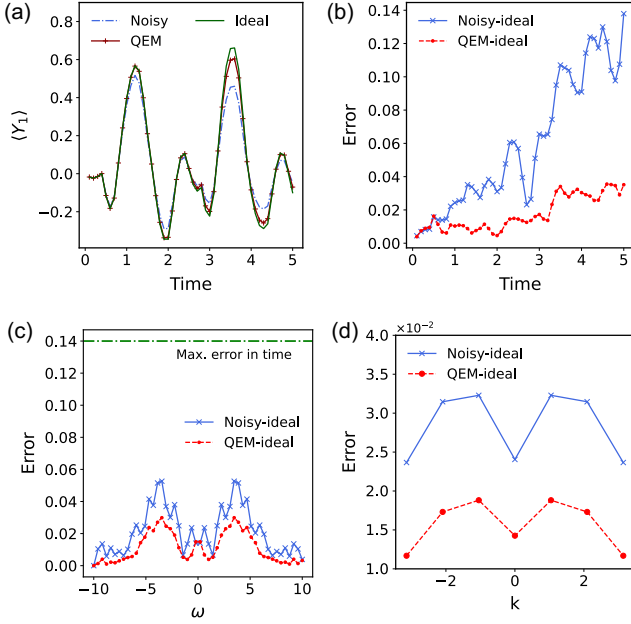


FIG. 4. **Noisy and error-mitigated time dynamics of the spectroscopy protocol.** **a** Dynamics of the observable expectation value $\langle Y_i \rangle$ at site $i = 1$. The figure shows the results of the noisy (with noise rate $p = 0.005$), the error mitigated and the ideal cases for a 7-site Ising model. **b** Root mean square error (RMSE) of the noisy and the error mitigated results in the time domain. **c** Error of the noisy and error mitigated spectrum in the frequency domain. The green line represents the maximum value of the error in the time domain as a reference. **d** Error in the k -space.

expressed as

$$H_{\text{BH}} = -J \sum_i \left(\hat{a}_i^\dagger \hat{a}_{i+1} + \text{h.c.} \right) + \frac{U}{2} \sum_i \hat{n}_i (\hat{n}_i - 1),$$

$$H_{\text{FH}} = -t \sum_i \left(\hat{c}_i^\dagger \hat{c}_{i+1} + \text{h.c.} \right) + U \sum_i \hat{n}_{i\uparrow} \hat{n}_{i\downarrow},$$

where \hat{a}_i and \hat{a}_i^\dagger (\hat{c}_i and \hat{c}_i^\dagger) are the bosonic (fermionic) annihilation and creation operators at the site i , respectively, and \hat{n}_i is the number operator acting on site i . In what follows, we examine whether our method does indeed replicate the true excitation spectra. For these types of particle systems (both bosons and fermions), we consider local perturbation by taking or adding particles to the site that we want to perturb. In this case, we remove all the particles in the central site of the chain. It is easy to see that this operation is not unitary and does not conserve the particle number, though we can find the unitary counterpart of this operation.

For the Hubbard models, we find the ground state using DMRG, apply local perturbation, evolve the system under the Hamiltonian, and finally measure the expectation value of the number operator. The results for the bosonic chain with an average filling of $\bar{n} = 1.4$ and $U/J = 2$ and for the fermionic chain simulation with

$h/J = 2$ are shown in Supplementary Figure 7. In all the 1D simulations, we use bond dimension $\chi = 128$ and chains of up to $N = 51$ sites. For the 2D cases, we need to increase the bond dimension in some cases due to the non-local nature of the MPS when having to simulate an extra dimension. We consider 2D lattices of dimensions $L_x \times L_y$ where $L_x = L_y = 11$. The simulation result for the lattice model with nearest-neighbour interaction is shown in Supplementary Figure 8. The focus here is to test the effectiveness of the spectroscopic method in a proof-of-principle way.

Simulation results when considering device and statistical noise. Here, we include device and statistical noise in the simulation. As discussed in the main text, the total running time complexity in the presence of device noise is polynomial $\mathcal{O}(\text{poly}(\epsilon^{-1}))$ in order to achieve a given precision. For global depolarising noise, the noise effect on observable estimation can be analytically derived. Given the knowledge of the error model, we can obtain error-mitigated observable estimation by fitting the noisy results.

Next, we test the performance of the simple error mitigation strategy by considering a more practical setup with a depolarising noise model. Specifically, we introduce local depolarising noise after each gate, including both single- and two-qubit gates. We numerically verify the behaviour of this noise model by emulating the noisy quantum circuits, where we apply local depolarising noise after each gate. We run the circuit for a Trotter step with time interval δt followed by its inverse: $U(\delta t)U^\dagger(\delta t)$, which is just identity without noise, and repeat it for different times. In Fig. 3, we show the results of $\sum_i \langle Y_i \rangle$ with an increasing circuit depth. Fig. 3 indicates that the noisy results can be well-approximated by an exponential decay function aligning with Eq. (9). The fitting results for individual observable $\langle Y_i \rangle$ are provided in Supplementary Section II.1.

For the noisy simulation and its error mitigation, we consider the 1D Ising model considered in the main text with an additional term $h_z = 0.1$. We set the initial state the same as that in the main text, a maximum time evolution of $T = 5$ and the time interval $\delta t = 0.4$. Results for varying system sizes (up to 11 sites) and noise rates are provided in Supplementary Section II.1. We mitigate the noisy measurement outcomes by using the fitted exponential functions for each qubit. The results under different conditions (noisy, ideal, and error mitigated) are shown in both the time and frequency domains in Fig. 4. We observe that even this simple error mitigation strategy can improve the results, though error mitigation is still needed for more general types of noise. As expected, the algorithm demonstrates strong resilience to noise, allowing us to recover the spectrum even after noisy evolution. This explains why the error is significantly smaller either in the frequency domain or the momentum space.

Compilation into quantum gates and implementation on IBM quantum devices After some initial

tests on the available quantum devices, the Kolkata device performed consistently for this task and thus was selected for executing the quantum circuits. We selected up to 13 qubits with good readout fidelities and gate fidelities. We used the second-order Trotter formula to simulate the dynamics. The real-time dynamics are compiled into single-qubit Pauli rotation gates and CNOT gates. For the Heisenberg model, the time-evolution operator $e^{-it \sum_i (X_i X_{i+1} + Y_i Y_{i+1} + Z_i Z_{i+1})}$ will be realised by Trotter formulae. Each component $e^{-ix(X_i X_{i+1} + Y_i Y_{i+1} + Z_i Z_{i+1})}$ with time duration x can be realised by 3 CNOT gates as proposed by [66]. For instance, $e^{-ix(X_1 X_2 + Y_1 Y_2 + Z_1 Z_2)}$ can be realised by the following circuit,

$$R_z^{(1)}\left(\frac{\pi}{2}\right)\text{CNOT}_{2 \rightarrow 1}R_y^{(2)}\left(\frac{\pi}{2} - 2x\right)\text{CNOT}_{1 \rightarrow 2}$$

$$R_y^{(2)}\left(2x - \frac{\pi}{2}\right)R_z^{(1)}\left(\frac{\pi}{2} - 2x\right)\text{CNOT}_{2 \rightarrow 1}R_z^{(2)}\left(-\frac{\pi}{2}\right)$$

This saves more gates when compared to using a naive compilation which needs 6 CNOT gates.

DATA AVAILABILITY

Data generated during the current study can be found on GitHub at https://github.com/luciavilchez/probing_spec_features.

CODE AVAILABILITY

Codes developed in the current study and the relevant examples can be accessed on GitHub at https://github.com/luciavilchez/probing_spec_features.

-
- [1] S. Mukamel, *Principles of nonlinear optical spectroscopy*, no. 6 (Oxford University Press, USA, 1995).
- [2] S. W. Lovesey, *Theory of neutron scattering from condensed matter* (1984).
- [3] A. T. Boothroyd, *Principles of Neutron Scattering from Condensed Matter* (Oxford University Press, 2020).
- [4] J. Als-Nielsen, D. McMorrow, *Elements of modern X-ray physics* (John Wiley & Sons, 2011).
- [5] M. Knap, A. Kantian, T. Giamarchi, I. Bloch, M. D. Lukin, E. Demler, Probing real-space and time-resolved correlation functions with many-body Ramsey interferometry. *Physical review letters* **111**, 147205 (2013).
- [6] Y. Wan, N. Armitage, Resolving continua of fractional excitations by spinon echo in the 2d coherent spectroscopy. *Physical Review Letters* **122**, 257401 (2019).
- [7] M. Kowalewski, B. P. Fingerhut, K. E. Dorfman, K. Bennett, S. Mukamel, Simulating coherent multidimensional spectroscopy of nonadiabatic molecular processes: From the infrared to the x-ray regime. *Chemical reviews* **117**, 12165–12226 (2017).
- [8] C. Senko, J. Smith, P. Richerme, A. Lee, W. Campbell, C. Monroe, Coherent imaging spectroscopy of a quantum many-body spin system. *Science* **345**, 430–433 (2014).
- [9] P. Jurcevic, B. P. Lanyon, P. Hauke, C. Hempel, P. Zoller, R. Blatt, C. F. Roos, Quasiparticle engineering and entanglement propagation in a quantum many-body system. *Nature* **511**, 202–205 (2014).
- [10] A. Valdés-Curiel, D. Trypogeorgos, E. Marshall, I. Spielman, Fourier transform spectroscopy of a spin-orbit coupled Bose gas. *New journal of physics* **19**, 033025 (2017).
- [11] M. Dalmonte, B. Vermersch, P. Zoller, Quantum simulation and spectroscopy of entanglement Hamiltonians. *Nature Physics* **14**, 827–831 (2018).
- [12] S. R. Manmana, S. Wessel, R. M. Noack, A. Muramatsu, Time evolution of correlations in strongly interacting fermions after a quantum quench. *Physical Review B* **79**, 155104 (2009).
- [13] B. Yoshimura, W. Campbell, J. Freericks, Diabatic-ramping spectroscopy of many-body excited states. *Physical Review A* **90**, 062334 (2014).
- [14] P. Richerme, Z.-X. Gong, A. Lee, C. Senko, J. Smith, M. Foss-Feig, S. Michalakis, A. V. Gorshkov, C. Monroe, Non-local propagation of correlations in quantum systems with long-range interactions. *Nature* **511**, 198–201 (2014).
- [15] R. Menu, T. Roscilde, Quench dynamics of quantum spin models with flat bands of excitations. *Physical Review B* **98**, 205145 (2018).
- [16] C.-K. Lee, J. W. Zhong Lau, L. Shi, L. C. Kwek, Simulating energy transfer in molecular systems with digital quantum computers. *Journal of Chemical Theory and Computation* **18**, 1347–1358 (2022).
- [17] A. Miessen, P. J. Ollitrault, F. Tacchino, I. Tavernelli, Quantum algorithms for quantum dynamics. *Nature Computational Science* **3**, 25–37 (2023).
- [18] Y. Ge, J. Tura, J. I. Cirac, Faster ground state preparation and high-precision ground energy estimation with fewer qubits. *Journal of Mathematical Physics* **60**, 022202 (2019).
- [19] G. H. Low, I. L. Chuang, Hamiltonian simulation by uniform spectral amplification. *arXiv preprint arXiv:1707.05391* (2017).
- [20] C.-K. Lee, C.-Y. Hsieh, S. Zhang, L. Shi, Simulation of condensed-phase spectroscopy with near-term digital quantum computers. *Journal of Chemical Theory and Computation* **17**, 7178–7186 (2021).
- [21] G. H. Low, I. L. Chuang, Hamiltonian simulation by qubitization. *Quantum* **3**, 163 (2019).
- [22] K. Bharti, A. Cervera-Lierta, T. H. Kyaw, T. Haug, S. Alperin-Lea, A. Anand, M. Degroote, H. Heimonen, J. S. Kottmann, T. Menke, *et al.*, Noisy intermediate-scale quantum algorithms. *Reviews of Modern Physics* **94**, 015004 (2022).
- [23] J. Tangpanitanon, A. Megrant, Z. Chen, B. Chiaro, A. Dunsworth, *et al.*, Spectroscopic signatures of localization with interacting photons in superconducting qubits. *Science* **358**, 1175–1179 (2017).
- [24] L. Villa, J. Despres, L. Sanchez-Palencia, Unraveling the excitation spectrum of many-body systems from quantum quenches. *Physical Review A* **100**, 063632 (2019).
- [25] L. Villa, J. Despres, S. Thomson, L. Sanchez-Palencia, Local quench spectroscopy of many-body quantum systems. *Physical Review A* **102**, 033337 (2020).

- [26] H. H. S. Chan, R. Meister, M. L. Goh, B. Koczor, Algorithmic shadow spectroscopy. *arXiv preprint arXiv:2212.11036* (2022).
- [27] M. L. Baez, M. Goihl, J. Haferkamp, J. Bermejo-Vega, M. Gluza, J. Eisert, Dynamical structure factors of dynamical quantum simulators. *Proceedings of the National Academy of Sciences* **117**, 26123–26134 (2020).
- [28] A. Chiesa, F. Tacchino, M. Grossi, P. Santini, I. Tavernelli, D. Gerace, S. Carretta, Quantum hardware simulating four-dimensional inelastic neutron scattering. *Nature Physics* **15**, 455–459 (2019).
- [29] Y. Matsuzaki, H. Hakoshima, K. Sugisaki, Y. Seki, S. Kawabata, Direct estimation of the energy gap between the ground state and excited state with quantum annealing. *Japanese Journal of Applied Physics* **60**, SBBI02 (2021).
- [30] I. Zintchenko, N. Wiebe, Randomized gap and amplitude estimation. *Physical Review A* **93**, 062306 (2016).
- [31] K. Sugisaki, K. Toyota, K. Sato, D. Shiomi, T. Takui, Quantum algorithm for the direct calculations of vertical ionization energies. *The Journal of Physical Chemistry Letters* **12**, 2880–2885 (2021).
- [32] K. Sugisaki, C. Sakai, K. Toyota, K. Sato, D. Shiomi, T. Takui, Bayesian phase difference estimation: a general quantum algorithm for the direct calculation of energy gaps. *Physical Chemistry Chemical Physics* **23**, 20152–20162 (2021).
- [33] H. Wang, S. Ashhab, F. Nori, Quantum algorithm for obtaining the energy spectrum of a physical system. *Physical Review A* **85**, 062304 (2012).
- [34] H. Wang, Quantum algorithm for obtaining the eigenstates of a physical system. *Physical Review A* **93**, 052334 (2016).
- [35] J. P. Stenger, G. Ben-Shach, D. Pekker, N. T. Bronn, Simulating spectroscopy experiments with a superconducting quantum computer. *Physical Review Research* **4**, 043106 (2022).
- [36] H.-Y. Huang, R. Kueng, J. Preskill, Predicting many properties of a quantum system from very few measurements. *Nature Physics* **16**, 1050–1057 (2020).
- [37] Y. Gu, Y. Ma, N. Forcellini, D. E. Liu, Noise-resilient phase estimation with randomized compiling. *Physical Review Letters* **130**, 250601 (2023).
- [38] P. Zeng, J. Sun, X. Yuan, Universal quantum algorithmic cooling on a quantum computer. *arXiv preprint arXiv:2109.15304* (2021).
- [39] L. Lin, Y. Tong, Heisenberg-limited ground state energy estimation for early fault-tolerant quantum computers (2021).
- [40] G. Wang, D. Stilck-França, R. Zhang, S. Zhu, P. D. Johnson, Quantum algorithm for ground state energy estimation using circuit depth with exponentially improved dependence on precision. *arXiv preprint arXiv:2209.06811* (2022).
- [41] M. Huo, Y. Li, Error-resilient monte carlo quantum simulation of imaginary time. *Quantum* **7**, 916 (2023).
- [42] Y. Yang, Y. Li, X. Xu, X. Yuan, Resource-efficient quantum-classical hybrid algorithm for energy gap evaluation. *Physical Review A* **109**, 052416 (2024).
- [43] Y. Dong, L. Lin, Y. Tong, Ground-state preparation and energy estimation on early fault-tolerant quantum computers via quantum eigenvalue transformation of unitary matrices. *PRX Quantum* **3**, 040305 (2022).
- [44] P. Jurcevic, P. Hauke, C. Maier, C. Hempel, B. Lanyon, R. Blatt, C. F. Roos, Spectroscopy of interacting quasiparticles in trapped ions. *Physical Review Letters* **115**, 100501 (2015).
- [45] P. Bleicker, G. S. Uhrig, Strong quenches in the one-dimensional fermi-hubbard model. *Physical Review A* **98**, 033602 (2018).
- [46] J. Vijayan, P. Sompet, G. Salomon, J. Koepsell, S. Hirthe, A. Bohrdt, F. Grusdt, I. Bloch, C. Gross, Time-resolved observation of spin-charge deconfinement in fermionic hubbard chains. *Science* **367**, 186–189 (2020).
- [47] L. Villa, S. Thomson, L. Sanchez-Palencia, Finding the phase diagram of strongly correlated disordered bosons using quantum quenches. *Physical Review A* **104**, 023323 (2021).
- [48] L. Villa, Out-of-equilibrium dynamics and quench spectroscopy of ultracold many-body quantum systems, Ph.D. thesis, Institut polytechnique de Paris (2021).
- [49] P. Jurcevic, H. Shen, P. Hauke, C. Maier, T. Brydges, C. Hempel, B. Lanyon, M. Heyl, R. Blatt, C. Roos, Direct observation of dynamical quantum phase transitions in an interacting many-body system. *Physical review letters* **119**, 080501 (2017).
- [50] X.-G. Wen, *Quantum field theory of many-body systems: From the origin of sound to an origin of light and electrons* (Oxford university press, 2004).
- [51] J. Bonča, S. A. Trugman, M. Berciu, Spectral function of the holstein polaron at finite temperature. *Physical Review B* **100**, 094307 (2019).
- [52] D. Jansen, J. Bonča, F. Heidrich-Meisner, Finite-temperature density-matrix renormalization group method for electron-phonon systems: Thermodynamics and holstein-polaron spectral functions. *Physical Review B* **102**, 165155 (2020).
- [53] F. Schrodi, P. Silvi, F. Tschirsich, R. Fazio, S. Montanero, Density of states of many-body quantum systems from tensor networks. *Physical Review B* **96**, 094303 (2017).
- [54] R. M. Nandkishore, W. Choi, Y. B. Kim, Spectroscopic fingerprints of gapped quantum spin liquids, both conventional and fractonic. *Physical Review Research* **3**, 013254 (2021).
- [55] E. Kökcü, H. A. Labib, J. Freericks, A. Kemper, A linear response framework for quantum simulation of bosonic and fermionic correlation functions. *Nature Communications* **15**, 3881 (2024).
- [56] P. Zeng, J. Sun, L. Jiang, Q. Zhao, Simple and high-precision hamiltonian simulation by compensating trotter error with linear combination of unitary operations. *arXiv preprint arXiv:2212.04566* (2022).
- [57] E. Knill, D. Leibfried, R. Reichle, J. Britton, R. B. Blakestad, J. D. Jost, C. Langer, R. Ozeri, S. Seidelin, D. J. Wineland, Randomized benchmarking of quantum gates. *Physical Review A—Atomic, Molecular, and Optical Physics* **77**, 012307 (2008).
- [58] J. J. Wallman, J. Emerson, Noise tailoring for scalable quantum computation via randomized compiling. *Physical Review A* **94**, 052325 (2016).
- [59] A. M. Dalzell, N. Hunter-Jones, F. G. Brandão, Random quantum circuits transform local noise into global white noise. *Communications in Mathematical Physics* **405**, 78 (2024).

- [60] J. Foldager, B. Koczor, Can shallow quantum circuits scramble local noise into global white noise? *Journal of Physics A: Mathematical and Theoretical* **57**, 015306 (2023).
- [61] K. Temme, S. Bravyi, J. M. Gambetta, Error mitigation for short-depth quantum circuits. *Physical review letters* **119**, 180509 (2017).
- [62] S. Endo, S. C. Benjamin, Y. Li, Practical quantum error mitigation for near-future applications. *Physical Review X* **8**, 031027 (2018).
- [63] J. Sun, X. Yuan, T. Tsunoda, V. Vedral, S. C. Benjamin, S. Endo, Mitigating realistic noise in practical noisy intermediate-scale quantum devices. *Physical Review Applied* **15**, 034026 (2021).
- [64] A. Gilyén, Y. Su, G. H. Low, N. Wiebe, *Proceedings of the 51st Annual ACM SIGACT Symposium on Theory of Computing* (2019), pp. 193–204.
- [65] B. Wu, J. Sun, Q. Huang, X. Yuan, Overlapped grouping measurement: A unified framework for measuring quantum states. *Quantum* **7**, 896 (2023).
- [66] A. Smith, M. Kim, F. Pollmann, J. Knolle, Simulating quantum many-body dynamics on a current digital quantum computer. *npj Quantum Information* **5**, 106 (2019).
- [67] J. Sun, Exploring quantum many-body systems from the viewpoints of quantum computing and spectroscopy, Ph.D. thesis, University of Oxford (2022).
- [68] A. A. Houck, H. E. Türeci, J. Koch, On-chip quantum simulation with superconducting circuits. *Nature Physics* **8**, 292 (2012).
- [69] I. M. Georgescu, S. Ashhab, F. Nori, Quantum simulation. *Reviews of Modern Physics* **86**, 153 (2014).
- [70] Z. Jiang, K. J. Sung, K. Kechedzhi, V. N. Smelyanskiy, S. Boixo, Quantum algorithms to simulate many-body physics of correlated fermions. *Physical Review Applied* **9**, 044036 (2018).
- [71] J. M. Martyn, Z. M. Rossi, A. K. Tan, I. L. Chuang, Grand unification of quantum algorithms. *PRX Quantum* **2**, 040203 (2021).
- [72] A. M. Childs, D. Maslov, Y. Nam, N. J. Ross, Y. Su, Toward the first quantum simulation with quantum speedup. *Proceedings of the National Academy of Sciences* **115**, 9456–9461 (2018).

ACKNOWLEDGMENTS

This work was initiated when J.S. was a postgraduate student at Oxford as part of his DPhil thesis, see Chapter 7 in [67]. L.V.E. and J.S. thank Louis Villa and Steven J. Thomson for discussions on tensor network simulation. J.S. thanks Weitang Li, Andrew Green, Pei Zeng, Chonghao Zhai, and Thomas Cheng for related and valuable discussions on this work. We acknowledge the use of the IBM quantum services for this work. The views expressed are those of the authors and do not reflect the official policy or position of IBM or the IBM quantum team. J.S. and M.S.K. acknowledge the Samsung GRC grant for financial support. V.V. thanks support from the Gordon and Betty Moore Foundation. J.S. thanks support from the Innovate UK (Project No.10075020). This work was also supported by EPSRC through EP/T001062/1,

the National Research Foundation of Korea (NRF) grant funded by the Korea government (MSIT) (No. RS-2024-00413957) and Schmidt Sciences, LLC. L.V.E is supported by the Clarendon Fund.

AUTHOR CONTRIBUTIONS

J.S., L.V.E., V.V., and A.B. conceived the idea. J.S. developed the theoretical aspect of the project. L.V.E. performed the numerical simulations with input from J.S.. J.S. performed simulations using IBM cloud services with input from M.S.K.. V.V., A.B. and M.S.K. supervised the project. J.S. and L.V.E wrote the manuscript. All the authors contributed to the discussion and writing up the manuscript.

COMPETING INTERESTS

The authors declare that there are no competing interests.

SUPPLEMENTARY INFORMATION FOR "PROBING SPECTRAL FEATURES OF QUANTUM MANY-BODY SYSTEMS WITH QUANTUM SIMULATORS"

Appendix A: Methods

This section elaborates on the framework and the spectroscopic method developed in the main text. In [Section A 1](#), we first prove that the two spectroscopic methods which introduce τ in different ways are equivalent. In [Section A 2](#), we analyse the mechanism by which our spectroscopy method is capable of detecting spectral properties. In [Section A 3](#), we study the estimation error of the transition energies under the finite circuit depth and sampling numbers, and provide the computational complexity of our method. In [Section A 4](#), we analyse the effect of algorithmic errors on our method.

1. The spectral detector and the equivalence of the two formalisms

In the main text, we consider $\tilde{g}(t) := \int_{-\infty}^{+\infty} p(\omega)e^{i\omega t}d\omega$ and its dual form $p(\omega) = \frac{1}{2\pi} \int_{-\infty}^{+\infty} \tilde{g}(t)e^{-i\omega t}dt$. The normalised function $g(t)$ is then introduced with the normalisation factor $c := \int_{-\infty}^{+\infty} |\tilde{g}(t)|dt$ and the phase factor $e^{i\theta t} := \tilde{g}(t)/(cg(t))$. We have $g(t) = \frac{1}{c} \int_{-\infty}^{+\infty} p(\omega)e^{-i\theta t}e^{i\omega t}d\omega$ and the dual form $p(\omega) = \frac{c}{2\pi} \int_{-\infty}^{+\infty} g(t)e^{i\theta t}e^{-i\omega t}dt$. If τ is introduced as a separate parameter that is irrelevant to the Fourier transform, it is straightforward to have

$$\tilde{g}_\tau(t) := \int_{-\infty}^{+\infty} p_\tau(\omega)e^{i\omega t}d\omega \quad (\text{A1})$$

and

$$p_\tau(\omega) = \int_{-\infty}^{+\infty} \tilde{g}_\tau(t)e^{-i\omega t}dt. \quad (\text{A2})$$

On the other hand, we can arrange that τ is coupled with ω in the Fourier transform, which is the way introduced in the main text. Then we have

$$g(t) = \frac{1}{c} \int_{-\infty}^{+\infty} p(\tau\omega)e^{-i\theta t}e^{i\tau\omega t}d(\tau\omega) \quad (\text{A3})$$

and

$$p(\tau\omega) = \frac{c}{2\pi} \int_{-\infty}^{+\infty} g(t)e^{i\theta t}e^{-i\tau\omega t}dt. \quad (\text{A4})$$

The following derivation shows the equivalence of these two ways. According to [Eq. \(A1\)](#), $\tilde{g}_\tau(t)$ takes the form of

$$\begin{aligned} \tilde{g}_\tau(t) &= \int_{-\infty}^{+\infty} p(\tau\omega)e^{i\omega t}d\omega \\ &= \frac{1}{\tau} \int_{-\infty}^{+\infty} p(\tau\omega)e^{i\omega\tau\frac{t}{\tau}}d(\tau\omega) = \frac{1}{\tau} \tilde{g}\left(\frac{t}{\tau}\right). \end{aligned} \quad (\text{A5})$$

The normalisation factor of $\tilde{g}_\tau(t)$ is given by

$$c(\tau) := \int_{-\infty}^{+\infty} |\tilde{g}_\tau(t)|dt = \int_{-\infty}^{+\infty} \frac{1}{\tau} |\tilde{g}\left(\frac{t}{\tau}\right)|dt = c. \quad (\text{A6})$$

We define a normalised function as

$$\text{Pr}(t, \tau) := \frac{|\tilde{g}_\tau(t)|}{c(\tau)} = \frac{1}{c} \frac{1}{\tau} |\tilde{g}\left(\frac{t}{\tau}\right)| = \frac{1}{\tau} g\left(\frac{t}{\tau}\right)$$

which can be expressed by $\text{Pr}(t, \tau) = \frac{1}{c(\tau)} \int_{-\infty}^{+\infty} p_\tau(\omega)e^{-i\theta t}e^{i\omega t}d\omega$, and the dual form is given by

$$p(\tau\omega) = \frac{c(\tau)}{2\pi} \int_{-\infty}^{+\infty} \text{Pr}(t, \tau)e^{i\theta t}e^{-i\omega t}dt. \quad (\text{A7})$$

According to Eq. (A7), we have

$$\begin{aligned}
p(\tau\omega) &= \frac{c(\tau)}{2\pi} \int_{-\infty}^{+\infty} \frac{1}{\tau} g\left(\frac{t}{\tau}\right) e^{i\theta t} e^{-i\omega t} dt \\
&= \frac{c(\tau)}{2\pi} \int_{-\infty}^{+\infty} g\left(\frac{t}{\tau}\right) e^{i\theta t} e^{-i\tau\omega \frac{t}{\tau}} d\left(\frac{t}{\tau}\right) \\
&= \frac{c}{2\pi} \int_{-\infty}^{+\infty} g(t') e^{i\theta t'} e^{-i\tau\omega t'} dt'.
\end{aligned} \tag{A8}$$

Here, we used that $g(t)$ and $g(\tau t)$ have the same phase factor. The above result indicates that Eq. (A7) can be converted to Eq. (A4) and hence the two formalisms are equivalent.

As discussed in the main text, there are two necessary requirements for inferring the transition energy $\Delta_{n',n} := E_{n'} - E_n$: (1) a sufficiently large coherence $\Gamma_{n',n}$, which can also be regarded a spectral weight and (2) a proper function $p(\omega)$ that ensures that $\Delta_{n',n}$ can be distinguished from other transition energies. The following strategy can be used in order to satisfy the first condition. We first prepare the initial state ρ as the ground state of the noninteracting system governed by H_0 . The interaction H_1 at $t = 0$ is then suddenly turned on. The state will be evolved under the Hamiltonian $H = H_0 + H_1$. In a weakly coupled regime, where the initial state ρ is close to the ground state $|0\rangle$ of H , the initial state can be expanded using the first-order perturbation as $\rho \simeq \rho^{00}|0\rangle\langle 0| + \sum_{n \neq 0} \rho^{0n}|0\rangle\langle n| + \rho^{n0}|n\rangle\langle 0|$. The state coherence ρ^{n0} is nonzero, which indicates that a transition between the eigenstate $|n\rangle$ and the ground state $|0\rangle$ is allowed. Therefore, by appropriately choosing the observable, we can in principle detect $\Delta_{n,0}$.

We can also probe the transition energy between the single-particle excited states $|n\rangle$ and $|n'\rangle$ in the weakly coupled system, similar to the way introduced in the main text. The transition could be expressed as $\langle n|\hat{O}|n'\rangle = \langle \mathbf{q}|\hat{O}|\mathbf{q} + \mathbf{k}\rangle$ where we represent the particle excitations in the momentum space, and the momentum selection rule is imposed. If the excitations are restricted to a single-particle manifold, we may choose an observable that conserves the particle number $\hat{O} = \sum_{\mathbf{p}, \mathbf{p}'} A_{\mathbf{p}, \mathbf{p}'} \hat{\gamma}_{\mathbf{p}}^\dagger \hat{\gamma}_{\mathbf{p}'}$. In this case, the observation is ensured to be nonzero since $\langle n|\hat{O}|n'\rangle = A_{\mathbf{q}, \mathbf{q} + \mathbf{k}}$. The derivation of the coherence $\Gamma_{n',n}$ was shown in Methods.

2. Extension of spectroscopic methods and the relation to the projection-based methods

To further understand why the engineered spectroscopy methods could be used to select the transition energies, we show that our method is closely related to the spectral-filter-based quantum algorithms, which effectively realise imaginary time evolution and can thus infer the eigenstates and eigenvalues. In this section, we analyse the mechanism by which our spectroscopy method is capable of detecting spectral properties. We will discuss the relation between our method and algorithmic cooling developed in [38].

Recall that we have introduced the function $G(t)$, which can be equivalently written in the Schrödinger picture as

$$G(t) = \langle \psi_0 | e^{iHt} \hat{O} e^{-iHt} | \psi_0 \rangle. \tag{A9}$$

This definition of the two-time correlation can be extended as

$$G(t_1, t_2) = \langle \psi_0 | e^{iHt_1} \hat{O} e^{-iHt_2} | \psi_0 \rangle. \tag{A10}$$

Let us define a weighted Fourier transform of $G(\tau t, \tau t')$ as

$$G(\omega, \omega') = \frac{c^2}{(2\pi)^2} \int_{-\infty}^{\infty} G(\tau t, \tau t') g(t) g(t') e^{i\theta t} e^{-i\theta t'} e^{-i\tau\omega t} e^{i\tau\omega' t'} dt dt'. \tag{A11}$$

We have

$$G(\omega, \omega') = \sum_{n, n'=0} \Gamma_{n',n} p(\tau(E_n - \omega)) p(\tau(E_{n'} - \omega')). \tag{A12}$$

Here, the function $p(\tau\omega)$ is the dual Fourier transform of $g(t)$ related by $p(\tau\omega) = \frac{c}{2\pi} \int g(t) e^{i\theta t} e^{-i\tau\omega t} dt$, which is the same as Eq. (A4).

Eq. (A12) indicates that the energies of $|n\rangle$ and $|n'\rangle$, which are originally connected by the energy selection rule, are now decoupled. Therefore, one can directly evaluate the energy instead of the energy gaps by tuning the parameters

ω, ω' . In particular, when we consider $\hat{O} = I$ and $t' = 0$, where

$$\begin{aligned}
G(\omega, 0) &= \frac{c}{2\pi} \int_{-\infty}^{\infty} G(\tau t, 0) e^{-i\tau\omega t} dt. \\
&= \frac{c}{2\pi} \int_{-\infty}^{\infty} \langle \psi_0 | e^{i\tau H t} | \psi_0 \rangle g(t) e^{-i\tau\omega t} dt \\
&= \frac{c}{2\pi} \sum_j |c_j|^2 \int_{-\infty}^{\infty} g(t) e^{i\tau(E_j - \omega)t} dt \\
&= \sum_j |c_j|^2 p(\tau(E_j - \omega)).
\end{aligned} \tag{A13}$$

To see why $G(\omega, 0)$ could select the eigenvalues, let us consider a matrix function acting on the Hamiltonian as

$$\hat{p}(H) := \sum_{i=0}^{N-1} p(E_i) |u_i\rangle \langle u_i|, \tag{A14}$$

where $p(h) : \mathbb{R} \rightarrow \mathbb{C}$ is a generic continuous-variable function determining the transformation of the spectrum of the Hamiltonian. One can verify that

$$G(\omega, 0) = \langle \psi_0 | \hat{p}(\tau(H - \omega)) | \psi_0 \rangle, \tag{A15}$$

which indicates that $G(\omega, 0)$ effectively realises the spectral filter operator \hat{p} on the initial state. For instance, the projection operator could be $\hat{p}(\tau H) = e^{-\tau^2 H^2}$, which projects out the contribution of other eigenstates with an increasing τ .

The eigenvalue information associated with the initial state $|\psi_0\rangle$ be expressed by

$$P(\omega) = \sum_j |c_j|^2 \delta(\omega - E_j), \tag{A16}$$

and one can verify that

$$G(\omega, 0) = (p \star P)(\omega), \tag{A17}$$

which is because

$$(p \star P)(\omega) = \int_{-\infty}^{\infty} p(t) P(\omega - t) dt = \sum_j |c_j|^2 \int_{-\infty}^{\infty} \delta(\omega - E_j - t) dt = \sum_j |c_j|^2 p(E_j - \omega). \tag{A18}$$

Note that the method in [55] could be regarded as a special case of our method when taking the filter operator to be an identity. They mainly discussed the dynamics simulation (rather than the spectroscopic feature estimation) within a linear response framework. Beyond the linear response regime, our method could be applicable to detect nonlinear spectroscopic features. Spectroscopic signatures appearing in nonlinear response can be found in [54]. For example, we can apply perturbations three times and obtain the higher order time correlation functions, similarly to the 2D coherent spectroscopy. We can resolve the continuum of the excitation spectrum by analysing the nonlinear susceptibility [6]. It is worth noting that their method for simulating the dynamics of bosonic and fermionic systems could be employed in this context.

3. Analysis of the algorithmic error and resource requirement

In this section, we provide proof for Lemma 1 and Lemma 2 in Methods.

Proof. (of Lemma 1)

When ω is close to Δ_j satisfying $|\omega - \Delta_j| \leq 0.5\varepsilon$, we have

$$\Gamma_j - G(\omega) \leq (1 - p(\tau(\Delta_j - \omega)))\Gamma_j + \max_{i \neq j} p(\tau(\Delta_i - \omega)) \leq (1 - e^{-\tau^2(0.5\varepsilon)^2})\Gamma_j + 0.05\tau^2\varepsilon^2\Gamma_j \leq 0.3\tau^2\varepsilon^2\Gamma_j. \tag{A19}$$

The second inequality uses the following fact that the inequality

$$\max_{i \neq j} p(\tau(\Delta_i - \omega)) \leq e^{-\tau^2(0.9\gamma)^2} \leq 0.05\tau^2\varepsilon^2\Gamma_j, \quad (\text{A20})$$

holds when $\tau = \frac{1}{0.9\gamma} \sqrt{\ln\left(\frac{20}{\varepsilon^2\Gamma_j}\right)} \geq 1$ and $\varepsilon \leq 0.2\gamma$. Thus the first inequality in Eq. (14) in Lemma 1 holds.

On the other hand, the quantity $\Gamma_j - G(\omega)$ can be lower bounded by

$$\begin{aligned} \Gamma_j - G(\omega) &\geq (1 - p(\tau(\Delta_j - \omega)))\Gamma_j - \max_{i \neq j} p(\tau(\Delta_i - \omega)) \\ &\geq (1 - e^{-\tau^2\varepsilon^2})\Gamma_j - e^{-\tau^2(0.9\gamma)^2} \\ &\geq 0.85\tau^2\varepsilon^2\Gamma_j - 0.05\tau^2\varepsilon^2\Gamma_j = 0.8\tau^2\varepsilon^2\Gamma_j. \end{aligned} \quad (\text{A21})$$

In the second inequality, we used the fact that $|\Delta_i - \omega| \geq 0.9\gamma$ for $i \neq j$. The third inequality $e^{-\tau^2\varepsilon^2} \leq 1 - 0.85\tau^2\varepsilon^2$ holds when $\tau\varepsilon < 1/2$, which can be achieved when $\varepsilon \leq \tilde{\mathcal{O}}(\gamma(\ln\Gamma_j^{-1})^{-\frac{1}{2}})$. \square

Lemma 2. *The estimation $\hat{\Delta}_j$ is related to the true transition energy Δ_j by $|\hat{\Delta}_j - \Delta_j| \leq \varepsilon$. with a failure probability of δ , when $\tau \geq \frac{1}{0.9\gamma} \sqrt{\ln\left(\frac{10}{\varepsilon^2\Gamma_j}\right)}$, the cutoff $T \geq 2\sqrt{2\ln(\sqrt{10}\tau^{-1}\varepsilon^{-1})}$ and the number of measurements $N_s \geq 200(\varepsilon^4\Gamma_j^2\tau^4)^{-1} \ln(4/\delta)$.*

Proof. Suppose we already have a rough estimation of Δ_j which lies in the range of $[\Delta_j^L, \Delta_j^R]$ with $\Delta_j^L = \Delta_j - \gamma/2$ and $\Delta_j^R = \Delta_j + \gamma/2$. Same as that in [38, 40], we consider a uniformly discretised grid with the grid resolution at least ε . With this consideration, the discretised frequency is given by $\omega_k = \Delta_j^L - 0.5\gamma + \frac{\gamma(k-1)}{M}$ for $k = 1, 2, \dots, M$ with $M = 2\lceil\gamma/\varepsilon\rceil + 1$ to ensure the resolution. It is worth noting that computing $\hat{G}^{(T)}(\omega)$ with different values of ω_k requires purely classical computing, and M is irrelevant to the measurement numbers N_s . One can use a much smaller grid size without demanding any additional quantum measurements.

The following shows that the transition energy can be estimated within a certain precision given the resources listed in Lemma 2. With the grid defined above, the estimation is determined by

$$\hat{\Delta}_j = \operatorname{argmax}_k \hat{G}^{(T)}(\omega_k). \quad (\text{A22})$$

The question is whether the estimation has a bounded error satisfying $|\hat{\Delta}_j - \Delta_j| \leq \varepsilon$.

The error due to a finite number of measurements can be bounded using the Hoeffding inequality. The estimator $\hat{G}^{(T)}(\omega)$ is related to ideal $G^{(T)}(\omega)$ by

$$|G^{(T)}(\omega) - \hat{G}^{(T)}(\omega)| \leq \Gamma_j\varepsilon_n, \quad \forall \omega \in \mathbb{R} \quad (\text{A23})$$

with a failure probability $\delta/2$ when $N_s = 2(\varepsilon_n\Gamma_j)^{-2} \ln(\frac{4}{\delta})$. Here we used the fact that $G_i^{(T)}(\omega) \leq 1$. Since the grid resolution is $\varepsilon/2$, there exists k_m , such that

$$|\omega_{k_m} - \Delta_j| \leq 0.5\varepsilon. \quad (\text{A24})$$

Combining the truncated spectral detector Eq. (16) (defined in Methods) and Eq. (A23), we have

$$\begin{aligned} \Gamma_j - \hat{G}^{(T)}(\omega_{k_m}) &\leq (\Gamma_j - G(\omega_{k_m})) + |G(\omega_{k_m}) - G^{(T)}(\omega_{k_m})| + |G^{(T)}(\omega_{k_m}) - \hat{G}^{(T)}(\omega_{k_m})| \\ &\leq 0.3\tau^2\varepsilon^2\Gamma_j + \varepsilon_T\Gamma_j + \Gamma_j\varepsilon_n \leq 0.5\tau^2\varepsilon^2\Gamma_j \end{aligned} \quad (\text{A25})$$

with a failure probability $\delta/2$. In the last inequality, we have set $\varepsilon_n = 0.1\tau^2\varepsilon^2$ and $\varepsilon_T \leq 0.1\tau^2\varepsilon^2$. The latter condition can be satisfied by setting $T \geq 2\sqrt{2\ln(\sqrt{10}\tau^{-1}\varepsilon^{-1})}$. This indicates that

$$\hat{G}^{(T)}(\hat{\Delta}_j) \geq \hat{G}^{(T)}(\omega_{k_m}) > (1 - 0.5\tau^2\varepsilon^2)\Gamma_j. \quad (\text{A26})$$

On the other hand, if the estimator determined by Eq. (A22) fails to give an accurate estimation up to ε , that is, $|\hat{\Delta}_j - \Delta_j| > \varepsilon$, then using Lemma 1 we have $\Gamma_j - G(\hat{\Delta}_j) \geq 0.8\tau^2\varepsilon^2\Gamma_j$. We have

$$\begin{aligned} \Gamma_j - \hat{G}^{(T)}(\hat{\Delta}_j) &\leq (\Gamma_j - G(\hat{\Delta}_j)) + |G(\hat{\Delta}_j) - G^{(T)}(\hat{\Delta}_j)| + (|G^{(T)}(\hat{\Delta}_j) - \hat{G}^{(T)}(\hat{\Delta}_j)|) \\ &\geq 0.8\tau^2\varepsilon^2\Gamma_j - \varepsilon_T\Gamma_j - \varepsilon_n\Gamma_j \geq 0.6\tau^2\varepsilon^2\Gamma_j \end{aligned} \quad (\text{A27})$$

with a failure probability $\delta/2$. The truncated estimator thus can be bounded

$$\hat{G}^{(T)}(\hat{\Delta}_j) \leq \Gamma_j(1 - 0.6\tau^2\varepsilon^2), \quad (\text{A28})$$

which violates Eq. (A26). Consequently, the assumption does not hold, which in turn proves that $|\hat{\Delta}_j - \Delta_j| \leq \varepsilon$ with a failure probability at most δ . \square

4. Coherent error effect in transition energy estimation

Our proposal relies on the measurement of $\hat{O}(t)$, which essentially requires the realisation of e^{-iHt} . The implementation by using product formulae will introduce a coherent Trotter error. By way of illustration, let us consider a simplified lattice model, whose Hamiltonian consists of two non-commutative terms as $H = H_1 + H_2$. The first-order Trotter formula reads

$$S_1(t) = e^{-itH_2}e^{-itH_1} = e^{-itH_{\text{eff}}} \quad (\text{A29})$$

where H_{eff} has an explicit form as $H_{\text{eff}} = H + \frac{1}{2}[H_1, H_2] + \dots$ by the Baker–Campbell–Hausdorff expansion. We can find that this algorithmic error brings about a perturbation to the original Hamiltonian which can be formally represented as $H_{\text{eff}} = H + \delta H$. The spectral features that we can actually probe are those of the new Hamiltonian.

Let us denote the eigenbases of the new effective Hamiltonian as $\{|\nu\rangle\}$. The quantity $G(\omega)$ becomes

$$G(\omega) = \sum_{\nu', \nu} \Gamma_{\nu', \nu} p(E_{\nu'} - E_{\nu} - \omega). \quad (\text{A30})$$

In the case of a lattice model which preserves the translation invariance, the new Hamiltonian also conserves translation invariance, that is, $\hat{\mathbf{P}}|\nu\rangle = \mathbf{p}_{\nu}|\nu\rangle$. The observable expectation is given by $\langle \nu | \hat{O}(\mathbf{x}) | \nu' \rangle = e^{i(\mathbf{p}_{\nu'} - \mathbf{p}_{\nu})\mathbf{x}} \langle \nu | \hat{O} | \nu' \rangle$. In this case, ν' and ν are connected according to the momentum selection rule $\mathbf{k} = \mathbf{p}_{\nu'} - \mathbf{p}_{\nu}$, which is similar to the noiseless one. However, noise will result in a deviation in transition energies.

It is natural to examine the noise effect using perturbation theory. The eigenenergy has a deviation from the original one $E_{\nu'} = E_n + \delta E_n$ with $\delta E_n = \langle n | \delta H | n \rangle$. The first-order change in the n th eigenstate is related to the unperturbed one by $|\nu\rangle = |n\rangle + \sum_{m \neq n} A_{mn} |m\rangle$ with $A_{mn} = \Delta_{nm}^{-1} \langle m | \delta H | n \rangle$. The quantity $G(\omega)$ becomes

$$G(\omega) = \sum_{\nu', \nu} \Gamma_{\nu', \nu} p(E_{n'} - E_n + \delta E_{n'} - \delta E_n - \omega). \quad (\text{A31})$$

The resolved energy difference $E_{n'} - E_n + \delta E_{n'} - \delta E_n$ has a deviation from the original one. Nonetheless, the momentum selection rule still holds, which imposes $\mathbf{k} = \mathbf{p}_{\nu'} - \mathbf{p}_{\nu}$. Here the coherence $\Gamma_{\nu', \nu}$ is changed from $\Gamma_{n', n}$. Up to the first order, the coherence has a difference as

$$\begin{aligned} \Gamma_{\nu', \nu} &= \left(\rho^{n'n} + \sum_m A_{mn} \rho^{n', m} + \sum_m A_{mn}^* \rho^{m, n} \right) \left(\langle n | \hat{O} | n' \rangle + \sum_m A_{mn'} \langle n | \hat{O} | m \rangle + \sum_m A_{mn}^* \langle m | \hat{O} | n' \rangle \right) \\ &= \Gamma_{n', n} + \langle n | \hat{O} | n' \rangle \left(\sum_m A_{mn} \rho^{n', m} + \sum_m A_{mn'}^* \rho^{m, n} \right) + \rho^{n'n} \left(\sum_m A_{mn'} \langle n | \hat{O} | m \rangle + \sum_m A_{mn}^* \langle m | \hat{O} | n' \rangle \right) \end{aligned} \quad (\text{A32})$$

One can find that in addition to $\Gamma_{n', n}$, some eigenstates $|m\rangle$, which are absent in the original selection rule, also contribute to $G(\omega)$. In the case where translation invariance is broken, the momentum selection rules will be lifted and the dispersion becomes broadened. This is similar to that of disordered systems. We can similarly derive the deviation of the energy and the coherence. We leave more detailed derivation to dedicated readers.

Appendix B: Noise analysis, mitigation and resource requirements

As discussed in the main text, the error sources include (1) algorithmic error, (2) uncertainty error due to a finite number of measurements and (3) error due to imperfect quantum operations. The preceding sections have discussed the algorithmic error and the uncertainty error (which is an unbiased error). We have discussed the resource requirement for the circuit depth and the number of measurements to ensure the simulation accuracy up to precision ε . In this section, we will analyse the error effect due to device noise and its mitigation strategy.

1. General strategy

We first introduce a general quantum error mitigation (QEM) strategy developed in [63] based on probabilistic error cancellation, and discuss the resource cost when considering noise. In our protocol, we mainly need the implementation of e^{-iHt_i} with different time lengths t_i . With analogue quantum simulators, e^{-iHt_i} is directly implemented through engineering the Hamiltonian of controllable quantum hardware. When assuming a Markovian type of noise that appears due to unwanted coupling between the device and the environment, the time evolution could be described by the Lindblad master equation of the noisy state $\rho_N(t)$

$$\frac{d\rho_N(t)}{dt} = -i[H(t), \rho_N(t)] + \lambda\mathcal{L}[\rho_N(t)]. \quad (\text{B1})$$

In the above equation, $\mathcal{L}[\rho] = \frac{1}{2} \sum_k (2L_k \rho L_k^\dagger - L_k^\dagger L_k \rho - \rho L_k^\dagger L_k)$ represents the noise superoperator with error strength λ that describes the coupling with the environment. Common noise models include dephasing and damping types of noise, which can be described by local Lindblad terms [68, 69].

The main idea of probabilistic error cancellation [61, 62] is to apply a recovery operation to the noisy state, so that the noisy process is mitigated. Below we briefly the probabilistic error cancellation proposed in [63]. Specifically, the noisy evolution of Eq. (B1) can be represented as $\rho_N(t + \delta t) = \mathcal{E}_N(t)\rho_\alpha(t)$ within a small time step δt where $\mathcal{E}_\alpha(t)$ denotes the noisy channel within small δt . A recovery operation \mathcal{E}_Q is an operation that can approximately map the noisy evolution back to the noiseless one up to the first order as $\mathcal{E}_I(t) = \mathcal{E}_Q\mathcal{E}_N(t) + \mathcal{O}(\delta t^2)$. We can adopt a probabilistic way to effectively realise \mathcal{E}_Q . That is, we can decompose \mathcal{E}_Q into a linear sum of physical operators $\{\mathcal{B}_j\}$ (i.e. basis operators) $\mathcal{E}_Q = c \sum_j \alpha_j p_j \mathcal{B}_j$, with coefficients $c = 1 + \mathcal{O}(\lambda\delta t)$, $\alpha_j = \pm 1$, and a normalised probability distribution p_j . The cost is $\mathcal{O}(\exp(\lambda T_{\max}))$, and thus, the error mitigation is efficient as long as λT_{\max} is bounded. We could see that in order to effectively implement QEM, the total required time should be short – if the maximum time is short, then the number of measurements can be bounded. As the time complexity of our method is $\mathcal{O}(\log(1/\epsilon))$, the total running time is $\mathcal{O}(\text{poly}(1/\epsilon))$.

For a short time evolution, the QEM strategy can be run in a stochastic setting, and it works for both analogue and digital quantum simulators. The number of the basis operations required for performing error mitigation on average scales linear in time as $\mathcal{O}(\lambda T_{\max})$.

2. Error mitigation for global depolarising noise

Below, we use a simple example to illustrate the error mitigation process. In order to mitigate the error effect, we need to assume the noise type. Within a short time, a simple way is to consider a depolarising noise model: the state remains unaffected with probability $\lambda\delta t$ while becomes a mixed state with probability $1 - \lambda\delta t$, with noise strength characterised by λ . This noisy process can thus be described by

$$\mathcal{E}_{\delta t}(\rho) = (1 - \lambda\delta t)\rho + \lambda\delta t\rho_{\text{mix}} \quad (\text{B2})$$

where $\rho_{\text{mix}} = \frac{I}{2^N}$ is the maximally mixed state and I is the identity matrix as defined in the main text. We could see that the noisy time-evolved state can be described by

$$\rho(t) = \prod_{\delta t}^T (\mathcal{E}_{\delta t} \circ \mathcal{U}_{\delta t})(\rho) = \Lambda(t)^{-1} \mathcal{U}_t(\rho) + (1 - \Lambda(t)^{-1})\rho_{\text{mix}} \quad (\text{B3})$$

where we have defined $\mathcal{U}_t := U(\cdot)U^\dagger$ and $\Lambda(t) = e^{\lambda t}$. The overall action can be described by

$$\mathcal{E} \circ \mathcal{U}_t(\rho) = \Lambda(t)^{-1} \mathcal{U}_t \rho \mathcal{U}_t^\dagger + (1 - \Lambda(t)^{-1})\rho_{\text{mix}} \quad (\text{B4})$$

This can be understood by evolving the state under \mathcal{U} followed by a noise channel $\mathcal{E}(\cdot) = \Lambda(t)^{-1}(\cdot) + (1 - \Lambda(t)^{-1})\rho_{\text{mix}}$. The effective action of such a noise channel is a global depolarising noise. We can find the noise channel coupled with the unitary operator is only dependent on t . The expectation value of a Pauli operator is

$$\mathbb{E}\hat{o}_{\text{noisy}}(t) = \text{Tr}(\mathcal{E} \circ \mathcal{U}_t(\rho)) = \Lambda(t)^{-1} \mathbb{E}\hat{o}_{\text{ideal}}(t). \quad (\text{B5})$$

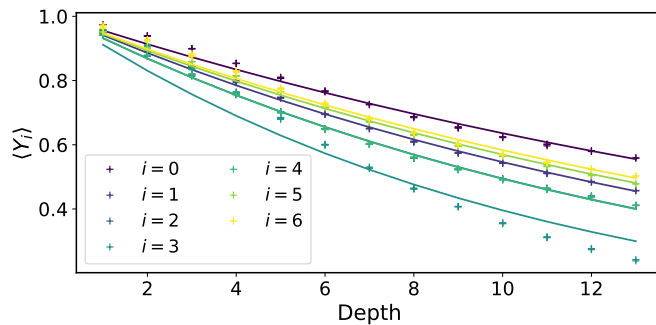


FIG. 5. Exponential fitting for individual qubits in the 7-site Ising model with local depolarising noise. Noise strength is set to $p = 0.005$. The setup is the same as that in Figure 5 in the main text.

As discussed in the main text, we can determine λ by fitting the noisy results with the ideal ones, in a similar spirit of randomised benchmarking. We run the circuit $(\tilde{\mathcal{U}}_{t/m} \circ \mathcal{U}_{t/m})^m = \mathcal{I}$ where $\tilde{\mathcal{U}}_{t/m} = U^\dagger(t/m)(\cdot)U(t/m)$, which should be an identity channel in the ideal case. In the presence of noise, it becomes

$$(\mathcal{E}_{t/m} \circ \tilde{\mathcal{U}}_{t/m} \circ \mathcal{E}_{t/m} \circ \mathcal{U}_{t/m})^m(\rho) = \Lambda(2t)^{-1}\rho + (1 - \Lambda(2t)^{-1})\rho_{\text{mix}} \quad (\text{B6})$$

when the noise is gate-independent. We could run it by fitting the result undergoing by the channel $(\mathcal{E}_{t/m} \circ \tilde{\mathcal{U}}_{t/m} \circ \mathcal{E}_{t/m} \circ \mathcal{U}_{t/m})^m$ with different t and m , such that this fitting process could be robust against state preparation and measurement errors.

Recall that each $\hat{o}(\tau t_i)$ is measured on a quantum computer. When doing error mitigation by scaling, the variance of $G(\omega)$ is amplified by factor $\Lambda(\tau|t_i|)$. In order to suppress the statistical error to ϵ , the number of measurements is amplified by the factor. The variance is related to $\Lambda(\tau \max_i |t_i|)$. Therefore, when the time is $\mathcal{O}(\log(1/\epsilon))$, the total time is $\mathcal{O}(\text{poly}(1/\epsilon))$. For other methods with the maximum time complexity being $\mathcal{O}(\text{poly}(1/\epsilon))$, the total time complexity is $\mathcal{O}(\exp(1/\epsilon))$.

It is worth noting that the above process can be regarded as an effective noise mitigation at the algorithmic level. This is in contrast to the case of general noise discussed in Section B 1 where physical operations (chosen from the set $\{\mathcal{B}_j\}$) are required to mitigate the noise.

3. Numerical simulation

In this section, we provide additional simulation results to support the noise mitigation strategies proposed in the main text. Specifically, we display fittings results for each qubit, results for different noise rates, and results for larger system sizes.

In the main text, we demonstrated that the average expectation value $\sum_i \langle Y_i \rangle$ can be approximated by an exponential decay function. In Fig. 5, we present the fitting results for the individual expectation value in the 7-site Ising model with $h_z = 0.1$. For each qubit i , the observable $\langle Y_i \rangle$ is fitted using an exponential decay function, with high predictive power $R \geq 0.98$. These individual fittings serve as the basis for our error mitigation strategy, showing that each qubit noisy measurement outcomes can be corrected effectively using these exponential functions. We note that this fitting strategy may be less effective for more general types of noise, and thus, we need error mitigation to obtain reliable results.

In Fig. 6, we show the results for the same 7-site Ising model with a lower noise rate $p = 0.001$. The figure presents the time dynamics and frequency domain analysis under different conditions: noisy, error mitigated, and ideal (noiseless). The QEM protocol continues to perform well in mitigating the noise effect, with observable errors reduced both in the time and frequency domains. These results indicate that our spectroscopic protocol maintains effective across different noise rates. To validate the scalability of our method, Fig. 7 shows the results for an 11-site Ising model with noise rate $p = 0.004$. We follow the same procedure as outlined above. The fitting (a), time dynamics (b) and time domain errors (c) are shown in Fig. 7 with the noisy, error-mitigated, and ideal cases. The results highlight that the QEM approach continues to be effective even for relatively larger system sizes.

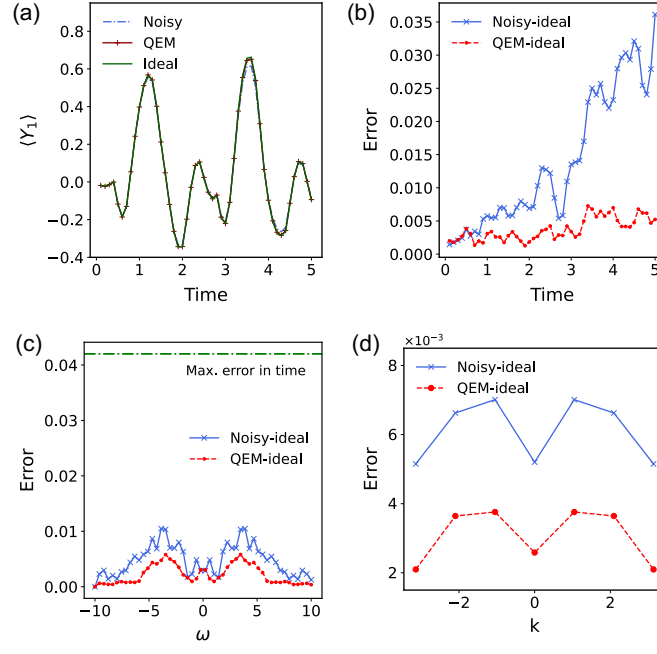


FIG. 6. Noisy and error-mitigated results for spectral property estimation. (a) Time evolution of the observable $\langle Y_i \rangle$ at site $i = 1$. The figure shows the results of the noisy (with noise rate $p = 0.001$), the error mitigated and the ideal (noiseless) cases for a 7-site Ising model. (b) RMSE of the noisy and the error-mitigated results in the time domain. (c) Error of the noisy and error mitigated spectrum in the frequency domain. The green line represents the maximum value of the error in the time domain to compare both results. (d) Error in the k-space.

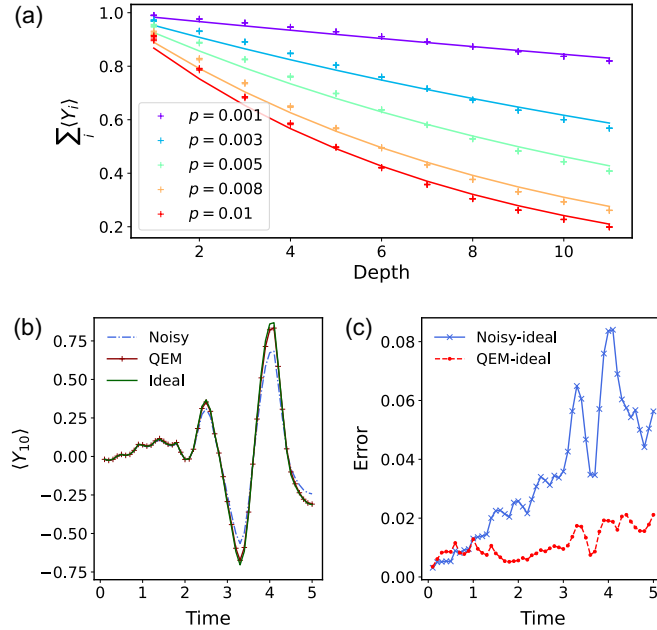


FIG. 7. Results of the error mitigation on an 11-site Ising model. (a) Average case fitting to exponential function with predictive power $R = 0.99$ for five different noise rates. (b) Time evolution of the observable $\langle Y_i \rangle$ at site $i = 10$. In this case, the noise rate is set at $p = 0.004$. (c) RMSE of the noisy and error mitigated results during the time evolution.

Appendix C: Comparison with other related works

Probing the spectral features of quantum systems is a highly active area of research that has attracted increasing attention. Numerous studies have been conducted in this direction. In this section, we compare our work with several representative studies in the field.

To begin with, we summarise the key elements of our method. This work concerns the central components in probing the transition energies and excitation spectra. The key elements in the spectroscopic method include how the initial state and the observable can be found to observe the transition energies, and whether spectral features can be virtually probed within a short time length. For the first one, we consider an initial state that contains a branch of excitations that we want to probe and we require a nonvanishing $\langle n|\hat{O}|n'\rangle$ to observe the transition between $|n\rangle$ and $|n'\rangle$. As widely accepted in the community, these requirements in general remain a challenge, though we have provided a few insights into finding observables in typical quantum systems. Additionally, as the measurement complexity in the estimation of multiple observables can be reduced by using classical shadow methods, we can extract the spectral information from a large number of observables, which is the key idea in [26]. For the second one, we have revealed a close relation between our method and the spectral filter methods, which naturally select the eigenenergies by projecting out the contributions from other eigenstates. Below we discuss related works from different aspects.

1. Scattering spectroscopy experiments and simulation of the experiments

It is interesting to discuss the similarities and differences between our method and conventional spectroscopy techniques. Both are capable of obtaining the energy excitation spectrum of a quantum system, but are different from operational perspectives. We first provide a brief introduction to spectroscopy. Experimental spectroscopy is a state-of-the-art probe approach that is used to uncover complex quantum many-body behaviours. In magnetic neutron scattering, for example, neutrons interact with spins of electrons, and the intensity of the scattered neutrons reflects the magnetic response of electrons in the materials. This in turn carries certain information about the magnetic interaction in the materials being probed. The observable in inelastic neutron scattering [2, 3] is the dynamical structure factor $S(\mathbf{Q}, \omega)$, also known as the magnetic response function, which is related to a two-point unequal-time correlator

$$C(t, t') = \langle \hat{\mathbf{S}}_1(t) \hat{\mathbf{S}}_2(t') \rangle, \quad (\text{C1})$$

by the Fourier transform, where $\hat{\mathbf{S}}$ is a spin operator. In conventional spectroscopy, the observables are related to two-point unequal-time correlation functions $C(t, t')$ and the initial state is in its equilibrium. The two-point unequal-time correlator contains spectral information on the spin dynamics of a many-body system. In a translationally invariant system, the dynamical structure factor $S(\mathbf{Q}, \omega)$ reaches its local maximum when the energy selection rule, as well as the momentum selection rule, are both satisfied. In a spectroscopic experiment, consequently, we usually track the peak of intensities in the neutron scattering spectrum, from which we can infer the energy dispersion. Some degrees of freedom in engineering the system are possible in spectroscopy experiments, such as through the application of an external electric or magnetic field. Nevertheless, the cost is huge because of the extreme experimental conditions and the high requirements in synthesising pure materials (pure in the sense that there are not many purities and the interactions types are clear).

Several works considered simulations of spectroscopy [16, 20], which is based on the simulation of the two-point unequal-time correlation function given by Eq. (C1). A drawback of the simulated spectroscopy is that it inherits the limitation of spectroscopy experiments and does not overcome it. In addition, in order to measure the unequal-time correlation function, a Hadamard-test circuit (a controlled time evolution) is usually required. As mentioned before, in the spectroscopy experiment or its simulation, the samples to be probed are in their equilibrium state, and thus, the information is restricted to the diagonal form. An advantage of our method is that because our initial state is not a steady state, and thus it can probe the energy difference between different excited states. In terms of implementation, they need one ancilla qubit that controls the rest of the qubits. In contrast, there is no overhead in compiling the non-local gate in our protocol and thus for lattice models, the depth within each time step is $\mathcal{O}(1)$.

In our work, the transition between different excited states can be probed given that the coherence is nonzero. One contribution of this work is to analyse how to choose the initial state and the observables in a physics-inspired way. This is rarely discussed in existing works. For example, in a recent paper [55], they assumed that the ground state could be prepared as the initial state, although they argued that this is not the scope of their work. As indicated by the complexity conjecture, the ground state and the thermal state are hard to prepare.

Our method is not restricted to the implementation in an analogue way. Indeed, our method is more versatile and can be useful when FTQC is advent. The reason why the method developed in this work can go beyond pure analogue

quantum simulation is twofold. The first is about the initial state preparation, and the second one is the the versatility in the time evolution. To see this point concretely, we give a class of examples of which analogue quantum computers may be hard to probe. Let us start with a model Hamiltonian for superconductivity. Because of the large numbers of particles involved, the fluctuations in the number of Cooper pairs should be small, which suggests a mean-field approximation to the BCS Hamiltonian. The BCS Hamiltonian becomes quadratic, which reads

$$H = \sum_{k,\sigma} \epsilon_k \hat{c}_{k,\sigma}^\dagger \hat{c}_{k,\sigma} + \sum_k \left(\Delta_k \hat{c}_{k,\uparrow}^\dagger \hat{c}_{-k,\downarrow}^\dagger + \Delta_k^* \hat{c}_{-k,\downarrow} \hat{c}_{k,\uparrow} \right) \quad (\text{C2})$$

where the irrelevant constant is removed. Analogue simulators can hardly simulate this type of Hamiltonians (e.g. its time evolution), which do not conserve particle numbers. However, since it is bi-linear in terms of creation and annihilation operators, the Hamiltonian can be diagonalized. Specifically, by using a Bogoliubov transformation, this Hamiltonian can be transformed into a diagonal form $H = \sum_{k,\sigma} \omega_k \hat{\gamma}_{k\sigma}^\dagger \hat{\gamma}_{k\sigma}$ where $\hat{\gamma}_{k\sigma}^\dagger$ and $\gamma_{k\sigma}$ are a new set of fermionic operators that satisfy the canonical anticommutation relations, and can be regarded as a rotated basis with respect to the original one. The rotated basis is related to the original basis by the unitary transformation as

$$\hat{\gamma}_j^\dagger = U \hat{c}_j^\dagger U^\dagger \quad (\text{C3})$$

where $j = (k, \sigma)$ and U is a unitary operator which does not conserve particle numbers. As discussed in quantum computing literature by Google's team [70], this unitary operator can be decomposed into local operators and thus can be implemented easily on quantum computers.

For the interacting case, we can prepare the initial state with a single quasiparticle excitation,

$$|\psi_0\rangle = \hat{\gamma}_j^\dagger |\text{vac}\rangle = U \hat{c}_j^\dagger |\text{vac}\rangle. \quad (\text{C4})$$

Although $\hat{\gamma}$ is not the previous operator, it can be implemented with a unitary transformation to the original basis. They also satisfy the canonical anticommutation relations. To prepare the initial state given by Eq. (C4), we only need to apply a unitary operator to an easy-to-prepare state. Eq. (C4) could serve a good initial state when the quasiparticle picture still holds. The Hamiltonian evolution can be realised by using Trotterisation or a random sampling way that is introduced in the main text.

Our method can be used to simulate the features of linear response, which is one application of the method presented here. The dynamics simulation methods for bosonic and fermionic systems introduced in [55] can be directly employed within our framework. Beyond the scope discussed in [55], we have discussed the conditions for designing the initial state and the complexity of exploring the spectral features.

2. Engineered spectroscopy methods

Finally, we compare our method to engineered spectroscopy methods, in particular Refs. [8, 13, 44]. It has been shown that nonequilibrium dynamics after a global quench [24, 44] or a local quench [25] could unveil certain excitation spectra, which has been termed quench spectroscopy. The basic idea is that quench will drive the initial stationary state out of equilibrium and generate low-lying quasiparticle excitations. The excitation spectrum can thus be obtained by measuring a properly chosen observable. For instance, the basic protocol of local quench spectroscopy for a lattice model with translation invariance is that we first initialise the system in its ground state, then apply a local operation to a single lattice site, and finally measure the dynamics of a local observable, which was initially proposed in [25]. It is worth noting that the 'local quench' in the original paper may stretch the conventional meaning of quench. Quench usually refers to a process where parameters in the Hamiltonian are changed in time, and usually the time scale for the change of parameters is very fast. For example, a system is prepared as an eigenstate of a Hamiltonian H_0 at $t < t_0$, while at time t_0 , the system is evolved dynamically under a different Hamiltonian $H_0 + H_1$. A more accurate description of 'local quench' in the protocol in [25] could be 'local perturbation'.

Let us consider a one-dimensional transverse field Ising model with,

$$H = \sum_{i < j \leq N} J_{ij} \hat{\sigma}_i^x \hat{\sigma}_j^x + h \sum_{j \leq N} \hat{\sigma}_j^z, \quad (\text{C5})$$

where $\hat{\sigma}_i^\alpha$ ($\alpha = x, y, z$) is a Pauli operator on the i th site, J_{ij} is the strength of spin-spin coupling between the i th and j th site. Ref. [44] considered a strong field case $h \gg \max J_{ij}$, in which the energy spectrum of H is split into $N + 1$ decoupled subspaces spanned by different excitation numbers. Below we briefly review the proposal in [44]. The Hamiltonian H conserves the total excitations numbers $\hat{n} = \sum_j (\hat{\sigma}_j^z + 1)/2$. They proposed observation of quasiparticle

spectroscopy by engineering the initial state consisting of the particular quasiparticle excitations. More specifically, by rotating the spins on each site $|\theta_j\rangle = \cos(\theta_j)|0\rangle_j + \sin(\theta_j)|1\rangle_j$ where $|0\rangle_j$ represents a spin-up state, the initial state $|\psi_0\rangle = \otimes_{j=1}^N |\theta_j\rangle$ could be a good approximation of a superposition of the ground state and the eigenstate of H in the single-excitation subspace. To probe the single quasiparticle excitations E_k , the initial state is prepared as

$$|\psi_0\rangle \approx |0\rangle + \beta |k\rangle, \quad (\text{C6})$$

where β is a small constant, $|0\rangle$ is the ground state and $|k\rangle$ is the eigenstate with a momentum k . Specifically, as suggested in [44], the eigenstates can be written as $|k\rangle = \sum_{j=1}^N \tilde{A}_j^k |1\rangle_j \otimes_{i \neq j} |0\rangle_i$ where for nearest-neighbour couplings $\tilde{A}_j^k = \sqrt{2/(N+1)} \sin(kj\pi/(N+1))$. By setting $\theta_j = \tan^{-1}(\beta \tilde{A}_j^k)$, we have a tensor product state that is a good approximation of Eq. (C6). It is easy to verify that the state coherence $\langle 0|\psi_0\rangle \langle \psi_0|k\rangle = \beta$. For probing transitions between $|k\rangle$ and $|k'\rangle$, the authors prepared the state as

$$|\psi_0\rangle \approx |0\rangle + \beta(|k\rangle + |k'\rangle), \quad (\text{C7})$$

in which the state coherence $\langle k|\psi_0\rangle \langle \psi_0|k'\rangle = \beta^2$. The choice of the initial states and observables is a special case of our method as discussed in Methods.

Yoshimura *et al.* considered a time-dependent field $B = B(t)$, which is decreased from a large polarising field to a constant, to create excitations, a method termed diabatic-ramping spectroscopy [13]. The transition energies can be obtained by taking the Fourier transform of the observable dynamics. Senko *et al.* considered a similar strategy, which applies time-dependent field $B(t) = B_0 + B_p \sin(2\pi v_p t)$ for probing the energy spectrum of a weakly coupled system. At the basis of this method is the emergence of an energy resonance between $|n\rangle$ and $|n'\rangle$ when the frequency of the external field, v_p , matches the transition energies $|\Delta_{n',n}|$ [8]. The emergence of resonance at $v_p = |\Delta_{n',n}|$ could be understood by time-dependent perturbation theory. In addition to the above specific Ising model, spectroscopy protocols have demonstrated that excitations can be effectively created in cases of Bose-Hubbard models [23, 24], spin chains [8, 13, 44], topological systems [54], and disordered systems [47].

3. Quantum algorithms for eigenenergy estimation

Existing universal quantum algorithms for finding eigenstates and the associated eigenenergies [19, 30, 33, 34, 64, 71], such as quantum phase estimation and quantum signal processing, generally require a deep circuit with long-time controlled operations, which remains a challenge for near-term quantum hardware. More importantly, simply in terms of efficiency, having an experiment-friendly method to access the behaviours of materials without requiring too many experimental resources is desirable. Our method only requires the realisation of time evolution e^{-iHt} without reliance on any ancillary qubits, a basic and most promising application of quantum computing [72]. This is in contrast to many Hamiltonian simulation algorithms and variational dynamics simulations, which usually require controlled-unitary operations. Our method is therefore compatible with an analogue quantum simulator, and has the advantage of potentially being more robust against noise. The quantum circuit complexity of our method for transition energy estimation is shown to be logarithmic in precision, while maintaining to be polynomial when device noise is present.

Zintchenko *et al.* [30] proposed an ancilla-free spectral gap estimation method. The spectral gap information is extracted from the computational-basis measurement results $|\langle 0|U^\dagger e^{-iHt} U|0\rangle|^2$ with U drawn uniformly from the Haar-random measure, which is different from our work. Recently, Wang *et al.* proposed quantum algorithms for ground state energy estimation [40]. More specifically, they proposed using a Gaussian derivative function in the form of $p_\sigma(t) = -\frac{1}{\sqrt{2\pi\sigma^3}} t \exp(-\frac{t^2}{2\sigma^2})$ as a filter to estimate the ground state energy, where σ plays a similar role to τ^{-1} . They achieved a maximal time complexity which is logarithmic in ε and a total running time $\tilde{O}(\varepsilon^{-2})$. It is worth noting that for the Gaussian derivative function, when ω approaches E_j , the convolution function value will be close to zero, instead of reaching its maximum. This function is thus constrained to estimate the ground-state energy instead of transition energies. Another relevant work is by Huo and Li, which proposed the following filtering function, $f(t) = \frac{1}{\pi} \frac{\beta}{\beta^2 + t^2} e^{-\frac{\beta^2 + t^2}{2\tau^2}}$, a product of Lorentz and Gaussian functions [41]. However, we find that this function cannot achieve logarithmic dependence because of the sharp feature close to $t \rightarrow 0$, which results in a flat function after the Fourier transform.

Recently, there have been some related works built upon the basics of quantum mechanics that the spectral information is contained in dynamics. A representative work is the algorithmic shadow spectroscopy, which proposed to infer the energy difference by calculating the Fourier transform of the observable expectations under time evolution [26]. These methods based on post-processing time-dependent signals inherit the problem of these classical methods, that is, generally require an evolution time proportional to the inverse of precision. By contrast, our method considers

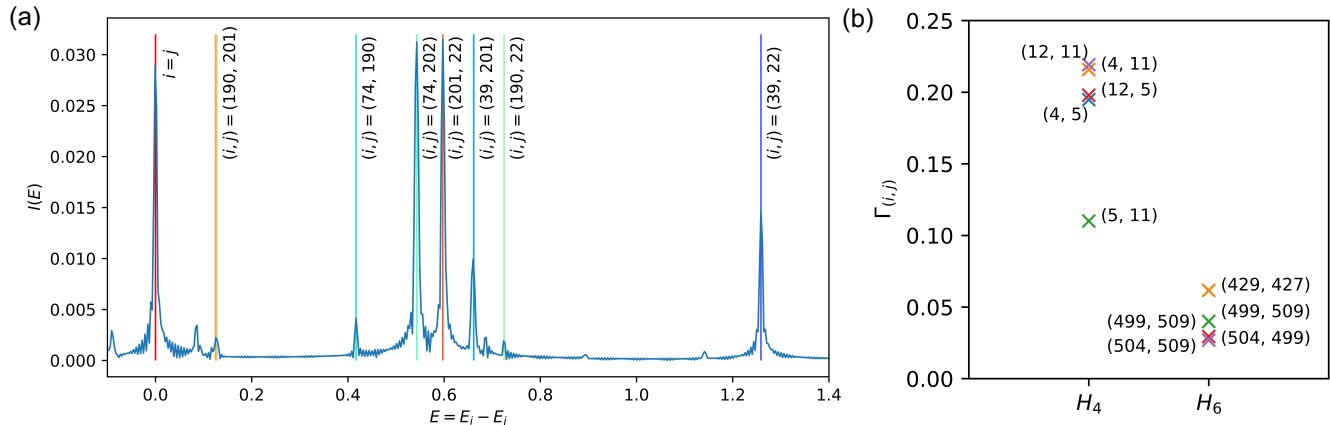


FIG. 8. (a) Transition energy spectra search of the H_4 molecule at the bond length $r = 3.0\text{\AA}$. The vertical lines show ideal transition energies, which are calculated by exact diagonalisation. The observable is chosen as a particle-conserving operator $\hat{c}_5^\dagger \hat{c}_7 + \hat{c}_5^\dagger \hat{c}_7$ with fermionic (creation) annihilation operator \hat{c} (\hat{c}^\dagger) with qubit numbering from zero. The cutoff for evaluating the integral is chosen as $T = 1$. (b) The largest coherences $\Gamma_{i,j}$ for H_4 and H_6 . The transitions are labelled by a pair (i, j) aside.

realising a spectral detector $G(\omega)$ to determine transition energies and has a theoretical guarantee for estimation accuracy. Gu *et al.* proposed an error-resilient algorithm for phase estimation without ancilla [37], similarly requiring long-time evolution. A detailed comparison between the two works could be interesting.

Appendix D: Numerical and experiment results

In this section, we discuss the implementation of our method in detail, and show more numerical and experimental results.

1. Transition energy estimation for molecular systems

In the main text, we showed the simulation of the energy differences for the LiH molecule, which is encoded in six qubits. The cutoff for evaluating the integral is chosen as $T = 2.5$. The observable is chosen as a particle-conserving operator $\hat{c}_0^\dagger \hat{c}_1 + \hat{c}_0 \hat{c}_1^\dagger$ with fermionic (creation) annihilation operator \hat{c} (\hat{c}^\dagger), which considers the transitions between low-lying excited states, in order to make $\langle n | \hat{O} | n' \rangle$ non-negligible. It is anticipated that more excitations will emerge when the molecule becomes complicated. We consider H_4 and detect its excitation spectrum using an approach similar to that in the main text. Fig. 8(a) shows the excitation spectrum of H_4 at the bond length $r = 3.0\text{\AA}$ encoded in eight qubits. Fig. 8(b) shows the coherence $\Gamma_{i,j}$ for H_4 and H_6 .

2. Excitation spectra of lattice models

In the main text, we presented the excitation spectra of the 11-site transverse-field Ising model and the 13-site Heisenberg model. The experiment was performed on the 27-qubit IBM Kolkata quantum device. The experimental results of the real-time dynamics on the IBM device are shown in Fig. 9. We present the simulation of the energy band for the Ising and Heisenberg chains with 51 qubit in Fig. 10. We set the parameters in the same way as Figure 3 in the main text. The numerical results have a good agreement with the dispersion relations in theory.

For the Hubbard models, we find the ground state using DMRG, apply local perturbation, evolve the system under the Hamiltonian, and measure the expectation value of the number operator. The results for the bosonic chain with an average filling of $\bar{n} = 1.4$ and $U/J = 2$ and for the fermionic chain simulation with $h/J = 2$ are shown in Fig. 11.

Finally, we apply MPS to study the excitation spectrum of 2D lattices of dimensions $L_x \times L_y$ where $L_x = L_y = 11$. The simulation result for the lattice model with nearest-neighbour interaction is shown in Fig. 12. Even though we can obtain the spectrum of the 2D system and examine how the trend adjusts to the expected result, the resolution is

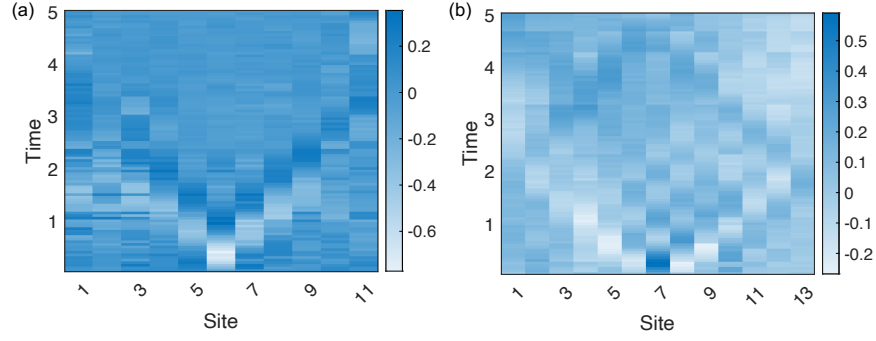


FIG. 9. (a,b) Time evolution of an 11-site transverse-field Ising model (a) and a 13-site Heisenberg model (b) executed on the IBM Kolkata quantum device.

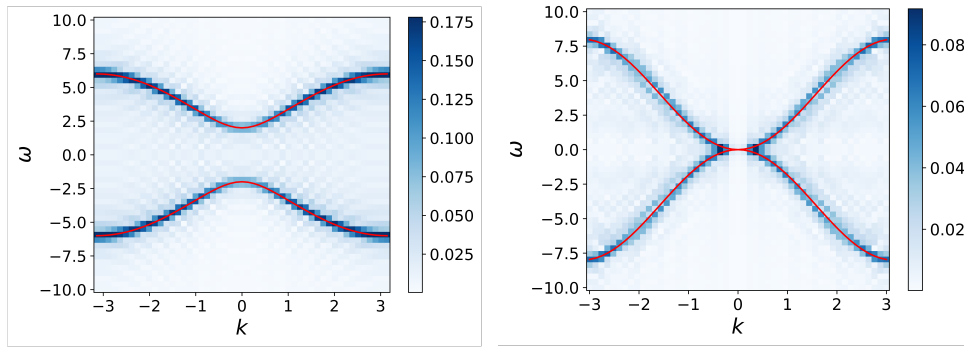


FIG. 10. Numerical simulation of the energy dispersions of lattice models. The excitation spectra of the Ising (a) and Heisenberg (b) model on a 51 site chain. The red lines represent the analytic results. The total evolution time is $T_{\text{tot}} = 10$.

limited by the significant computational complexity involved. One could improve the resolution by raising the number of sites, which, however, will significantly increase the time duration of classical simulations based on tensor networks.

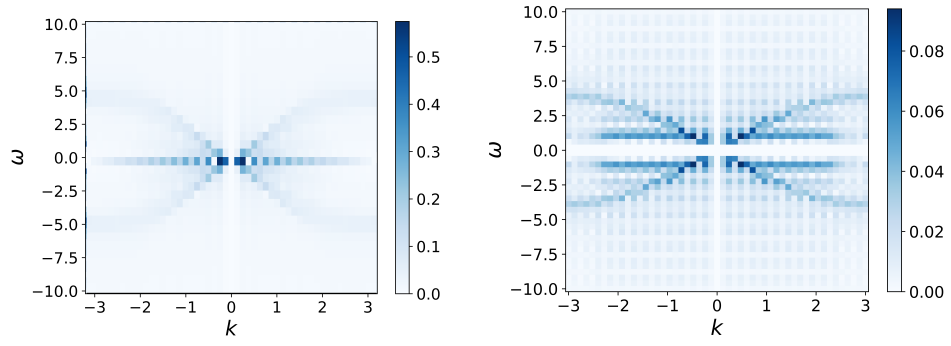


FIG. 11. Simulation of the Bose-Hubbard model for $U/J = 2$ (a), and the Fermi-Hubbard model $h/J = 2$ (b) for on a chain with $L = 49$ sites. The energy dispersion relations are shown.

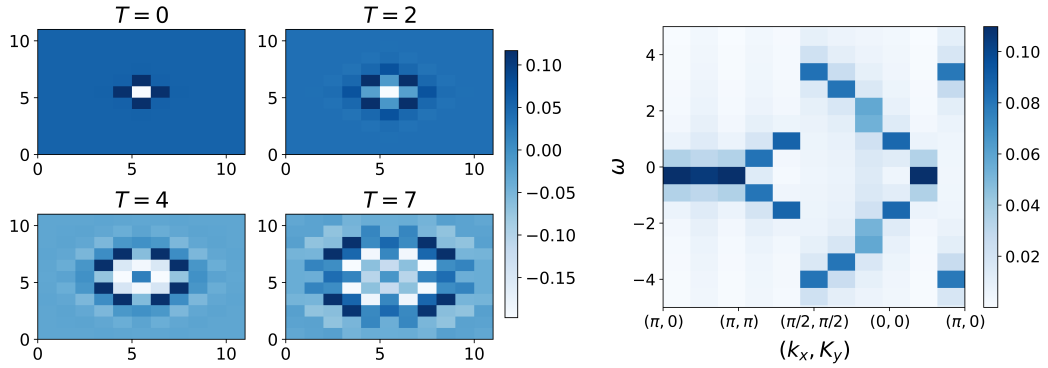


FIG. 12. Simulation of the Heisenberg model Hamiltonian applied on a square lattice with $L_x = L_y = 11$: (a) Evolution of the expectation value of the spin operator $\langle \sigma_i^y(t) \rangle$. (b) The normalized modulus of the spectral function.